Journal of Sound and Vibration (1993) **168**(2), 253–284

ENERGY FLOW VARIABILITY IN A PAIR OF COUPLED STOCHASTIC RODS

A. J. KEANE AND C. S. MANOHAR

University of Oxford, Department of Engineering Science, Parks Road, Oxford OX1 3PJ, England

(*Received* 18 *March* 1992, *and in final form* 11 *June* 1992)

Random variations in the transfer functions describing energy flows in a pair of coupled axially vibrating stochastic rods are considered. The material properties of the rods are modelled either as random variables or as random processes, and the consequent effects on the nature of the power receptance functions are studied by using Monte Carlo simulation techniques. The relevance of these results is discussed in the context of variability in average estimates obtained when using Statistical Energy Analysis (SEA) formalisms. The response statistics are shown to vary significantly with the details of the statistical modelling of the system, especially in the low and medium frequency ranges. Moreover, the confidence limits show no tendency to converge toward the mean with increasing frequency. Critical systems the responses of which deviate maximally from the average values are identified and attempts made to understand their nature.

1. INTRODUCTION

In the vibration of engineering structures subjected to high frequency excitation several modes of vibration can be expected to contribute to the response at any given frequency. A major problem in the analysis of such vibrations occurs in handling the extreme sensitivity of these natural modes of vibration to minor changes in specification of system parameters and details of the mathematical modelling of the system. Statistical Energy Analysis (SEA) makes allowance for this fact by treating the vibrating system as being drawn from a statistical ensemble of nominally similar systems [1]. The energy levels in individual subsystems are taken to be the principal response variables of interest and are calculated as averages across this ensemble. The actual structure under consideration is thought of as a member of the ensemble and the averaged response as a measure of its response. If these averaged responses are to be meaningfully employed in design practice, it is clearly desirable to establish measures of dispersion in the response variables and also to determine confidence levels associated with the estimated averages. Clearly, in such calculations one needs to describe the statistical ensemble of vibrating systems in greater detail than would be needed for the determination of the average response alone.

The first step in a systematic investigation of this problem involves deciding on the nature of the stochastic model to be employed for the vibrating system. In this context it may be noted that the statistical aspects of system modelling can be incorporated into the response calculations at basically two different levels. The first involves constructing appropriate models for the stochastic variability in material, geometric and topological properties of the vibrating system, followed by a free vibration analysis to determine the associated random natural frequencies and mode shapes. This information can then be incorporated into a forced response analysis. The second and somewhat simpler alternative

0022–460X/93/260253 + 32 $08.00/0

is to postulate directly stochastic models for the natural frequencies and mode shapes and use these in forced response calculations. This approach clearly bypasses the need to carry out a stochastic free vibration analysis, but its success depends on the accuracy of modelling the modal parameters. Consequently, the former approach is adopted here.

2. A BRIEF REVIEW OF EARLIER WORK

In the past, relatively few authors have considered the problem of determining measures of dispersion and confidence levels associated with the response levels in statistically defined vibrating structures. Notable among them are Lyon and Eichler [2], Lyon [1, 3], Fahy [4], Davies and Wahab [5], Davies and Khandoker [6] and Mohammed and Fahy [7]. The problem has also been discussed in a review paper by Hodges and Woodhouse [8].

In the paper by Lyon [3] an historical review of statistical modelling of vibrating structures and acoustical systems was presented. Also considered was the problem of calculating the statistics of power injected into single vibrating structures by narrow-band and broadband excitations plus the statistics of the response of the structure. The statistical modelling of the system was introduced at the eigensolution level. Thus, the natural frequencies of the system were modelled as a set of stationary Poisson points on the frequency axis, with the arrival rate given by the modal density of the structure. Consequently, distinct natural frequencies under this assumption became statistically independent and identically distributed uniformly in the frequency range of interest. The spacing between successive natural frequencies was, in turn, exponentially distributed. The mode shapes were treated as deterministic quantities. The point of application of the force was taken to be a random variable distributed uniformly over the domain of the structure. Based on these assumptions and using standard results from Poisson process theory, Lyon derived the mean and standard deviation of the power input to the structure. Furthermore, in order to calculate the confidence level associated with the estimated averages, a gamma probability density function was fitted to the power input using the calculated mean and standard deviation. Under the additional assumption that the point of forcing and the point of measurement are independent random variables, identically distributed uniformly over the domain of the structure, he also calculated the statistics of the structural response. Within a framework of similar assumptions, Lyon [1] also discussed the statistics and confidence intervals of energy levels and dynamical responses in connected structures.

The assumption of a Poisson process model for natural frequencies in these analyses results in considerable analytical simplicity. Nevertheless, it is an *ad hoc* assumption and it is not obvious whether the occurrence of natrual frequencies in engineering structures satisfy the postulates underlying the construction of Poisson processes. The effect of ignoring the random variability in mode shapes, especially at points of driving, coupling and measurement, is again not clear.

In this context, it may also be noted that a number of studies have been reported in the nuclear physics literature on the determination of energy levels associated with complex nuclei. In mathematical terms, these energy levels are calculated as the eigenvalues of matrices the elements of which are modelled as random variables; see the paper by Brody *et al.* [9], for a recent review. Lyon [3] has noted the possible relevance of these results to SEA applications. In particular, he considered non-Poissonian natural frequency spacing models which take into account the tendency of two neighbouring natural frequencies to repel each other. Similar views have also been expressed recently by Weaver [10].

3. THE PRESENT STUDY

In the present study the variability in energy flow characteristics in one-dimensional coupled structural configurations is considered. Several factors pertaining to the nature of excitation, coupling and subsystem properties can be expected to contribute to the variability in energy flow characteristics. Principally, these are (i) the spectrum and spatial variation of excitation, (ii) the coupling strength and location, (iii) the statistical variations in mass, stiffness and boundary conditions of the subsystems which in turn govern the variations in natural frequencies and mode shapes and (iv) the number of constituent subsystems. The present study is, however, largely focused on the details of the statistical modelling of subsystem properties and their consequent effect on the power flows. The system considered for study is constructed by coupling two axially vibrating rods at a single point through a linear, conservative spring. Two specific types of excitations, namely point harmonic forcing and a distributed rain on the roof type of excitation, are considered. The *physical* properties of the structure, namely the mass and stiffness, are modelled as random quantities. The ensemble of vibrating systems is simulated computationally by using Monte Carlo techniques. The power transmission calculations for individual realizations of the system are carried out based on the exact formulations derived by Davies [11] as developed further by Keane and Price [12]. The statistical properties of the response quantities of interest are then obtained by processing the ensemble of response variables. In particular, calculations are made for the mean, standard deviation, 5% and 95% probability levels and extreme values of the response variables. The validity of the simulation algorithm has also been checked by comparing simulation results with certain specific, exact analytical solutions. These analytical solutions have been developed recently by the present authors for the case of an axially vibrating stochastic rod [13]. It may be emphasized that the power transmission calculations for individual realizations are not based on any of the traditional SEA assumptions and, therefore, are uniformly valid over the entire frequency range of interest.

It is clear that there is no unique way of generating an ensemble of vibrating systems. Thus different randomization schemes adopted for generating these ensembles would, in principle, lead to different sets of solutions. While the results for the means may reasonably be assumed to be insensitive to these details of modelling, the same may not be true if one considers higher order statistics or the extremal behaviour of the response. A principal aim of the present study has been to investigate the effect of different randomization schemes on such response statistics.

In a simulation study dealing with the determination of deviations from average behaviour, it is clearly of interest to understand the nature of specific realizations of structural configurations which lead to extremal responses. The extrema of responses depend on the behaviour of the associated probability density function near the tails and hence are sensitive to the sample size used in simulation work. On the other hand, if interest is focused on the extremal behaviour alone, then it is much simpler to use numerical optimization schemes than Monte Carlo simulations to determine structural configurations which show such responses. This option has been adopted in the present study to determine "optimal" distributions of mass and stiffness properties along the length of a pair of coupled rods which lead to extreme responses under a prescribed excitation.

4. THE TWO-ROD SYSTEM

The system under consideration consists of a pair of axially vibrating rods which are mutually coupled at a point through a spring, the system configuration being illustrated

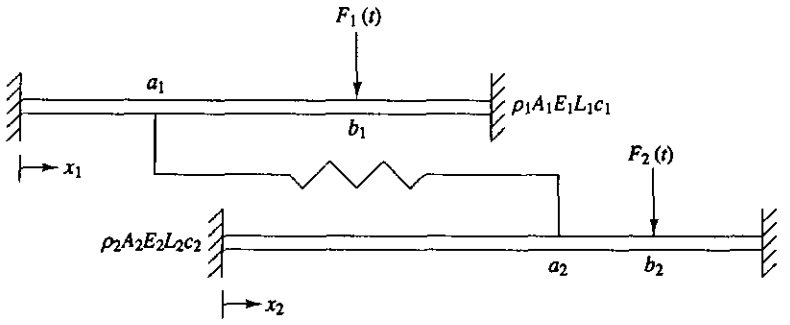

Figure 1. Two point spring coupled axially vibrating rods.

in Figure 1. The rods are assumed to have random material and/or geometrical properties. Specifically, the mass and/or stiffness properties of the individual rods are modelled either as random variables or as random processes. The rods are assumed to be viscously damped, with the damping coefficients being proportional to the masses. No restrictions are placed either on the magnitude of the damping or on the strength of the coupling spring. The external forces acting on the system are modelled as point harmonic excitation or as rain on the roof type of distributed forcing. The aim of the present study is to examine the probabilistic nature of the power flow characteristics in the system arising out of random fluctuations in the properties of the system. The response variables of interest are taken to be the steady state energy levels in the two systems, these variables in turn being described in terms of various system transfer functions. Of particular interest are the input power receptance function and the coupling power receptance function. The deterministic aspect of power transmission characteristics in this type of system has been studied by several authors [11, 14, 15], and the expressions for the desired receptance functions are reproduced here without detailed derivation. Thus, when two rods are coupled at $x_i = a_i$ and are excited by point forces $F_i(t)$ acting at $x_i = b_i$, $i = 1, 2$, the input power and coupling power receptances for the first rod are given, respectively, by

$$H_{11}(\omega) = (\omega^2 c_1/m_1) \sum_{i=1}^{\infty} (\psi_i(b_1)/|\phi_i|^2) + (\omega k_c/m_1^2) \operatorname{Im} \left\{ \frac{1}{\Delta} \left[\sum_{i=1}^{\infty} \psi_i(b_1)\psi_i(a_1)/\phi_i \right]^2 \right\}, \quad (1)$$

$$H_{12}(\omega) = \frac{\omega^2 k_c^2 c_2}{m_1^2 m_2 |\Delta|^2} \sum_{r=1}^{\infty} (\psi_r^2(a_2)/|\phi_r|^2) \left| \sum_{i=1}^{\infty} (\psi_i(b_1)\psi_i(a_1)/\phi_i) \right|^2. \quad (2)$$

Similarly, when the system is excited by distributed forces $F_i(x_i, t)$, $i = 1, 2$, of the rain on the roof type, the above receptances are given, respectively, by

$$H_{11}(\omega) = (\omega^2 c_1/m_1) \sum_{i=1}^{\infty} (1/|\phi_i|^2) + (\omega k_c/m_1^2) \operatorname{Im} \left\{ \sum_{i=1}^{\infty} (\psi_i^2(a_1)/\phi_i^2 \Delta) \right\}, \quad (3)$$

$$H_{12}(\omega) = \frac{\omega^2 k_c^2 c_2}{m_1^2 m_2 |\Delta|^2} \sum_{r=1}^{\infty} (\psi_r(a_2)/|\phi_r|^2) \sum_{i=1}^{\infty} (\psi_i^2(a_1)/|\phi_i|^2). \quad (4)$$

In these equations the summations over the indices i and r respectively denote summations over the modes of the first and second rods. The quantities ω_i and ψ_i are, respectively, the natural frequencies and the mode shapes. The quantities ϕ_i and Δ are given by

$$\phi_i = \omega_i^2 - \omega^2 + \mathrm{i} c_1 \omega \quad \text{and} \quad \Delta = 1 + (k_c/m_1) \sum_{i=1}^{\infty} (\psi_i^2(a_1)/\phi_i) + (k_c/m_2) \sum_{r=1}^{\infty} (\psi_r^2(a_2)/\phi_r). \quad (5, 6)$$

The mode shapes ψ satisfy the orthogonality conditions

$$\int \psi_i(x_1)\psi_j(x_1)\rho_1(x_1)\,dx_1 = m_1\delta_{ij}. \tag{7}$$

Here δ_{ij} denotes the Kronecker delta function. The quantities c_i, m_i and ρ_i, respectively, denote the coefficient of viscous damping, total mass and mass per unit length of the ith system. k_c is the coupling spring constant. The forces F_1 and F_2 are assumed to be statistically independent.

When the mass and/or stiffness properties of the individual rods are modelled as random quantities, the natural frequencies and mode shapes become random in nature. The receptance functions described above, in turn, become random processes. The aim of the present investigation is to obtain probabilistic descriptions of $H_{ij}(\omega)$, $i,j = 1, 2$, as functions of the probabilistic description of the mass and stiffness profiles of the individual rods. A general analytical solution to this problem is currently not possible. Estimates for the probability distribution function (PDF) of $H_{ij}(\omega)$ can, however, be easily obtained by using Monte Carlo simulation techniques. For this purpose, an ensemble of realizations of coupled rod systems is computationally simulated as per the stochastic model adopted for the mass and stiffness properties. For every realization of the pairs of rods, the natural frequencies and mode shapes are calculated for each of the individual rods and this information is incorporated into equations (1)–(4) to generate the ensemble of receptance functions. This ensemble is further processed to obtain the desired PDFs. Thus a crucial step in these calculations involves obtaining the natural frequencies and mode shapes of the simulated rods. When the mass and stiffness of the rods are modelled as *random variables*, each realization consists of rods with *uniform* properties. The eigensolutions of such rods are well known [16]. On the other hand, when the mass and stiffness properties are modelled as *random processes* each realization results in rods with *spatially varying* properties. In such cases, special means are needed to derive the natural frequencies and mode shapes of the rods.

5. EIGENSOLUTIONS OF NON-UNIFORM RODS

The eigenvalue problem of an axially vibrating fixed–fixed rod with length L, stiffness AE and mass per unit length ρ consists of determining the non-trivial solutions of the equation

$$\frac{d}{dx}\left[AE(x)\frac{dy}{dx}\right] + \omega^2\rho(x)y = 0, \tag{8}$$

subject to the boundary conditions

$$y(0) = 0, \qquad y(L) = 0. \tag{9}$$

In order to calculate the eigenvalues, consider the solution $y^*(x, \omega)$ of equation (8) under the *initial conditions*

$$y^*(0, \omega) = 0, \qquad (dy^*/dx)(0, \omega) = 1. \tag{10}$$

Notice that the equations (8) and (10) have a non-trivial solution for any arbitrary value of ω. The eigenvalues of equations (8) and (9) can, however, be defined in terms of $y^*(x, \omega)$. In fact, those ω's which satisfy the equation

$$y^*(L, \omega) = 0 \tag{11}$$

are the desired eigenvalues of equations (8) and (9). Thus, a root searching technique can be instituted to find the ω's which satisfy equation (11). These ω's can further be back-substituted into equation (8) to determine the eigenfunctions.

The study of $y^*(x, \omega)$ is facilitated if the non-uniform rod is idealized as a rod constructed out of p piecewise uniform sections with lengths l_m, stiffness AE_m and mass per unit length ρ_m, $m = 1, p$. This means that the continuous functions $AE(x)$ and $\rho(x)$ are approximated by a sequence of piecewise uniform functions. Within the mth subsection the solution is known to be given by

$$y^*(x_m, \omega) = Y_m \sin [\lambda_m x_m + \theta_m], \qquad 0 < x_m < l_m. \tag{12}$$

Here λ_m defines the local wave speed in the mth section and is given by

$$\lambda_m = \omega \sqrt{(\rho_m / AE_m)}. \tag{13}$$

The consideration of continuity of displacement and force at each junction leads to the conditions

$$\tan \theta_{m+1} = \sqrt{\frac{\rho_{m+1} AE_{m+1}}{\rho_m AE_m}} \tan (\lambda_m l_m + \theta_m)$$

and

$$\left(\frac{Y_{m+1}}{Y_m}\right)^2 = 1 + \left(\frac{\rho_m AE_m - \rho_{m+1} AE_{m+1}}{\rho_{m+1} AE_{m+1}}\right) \cos^2 (\lambda_m l_m + \theta_m). \tag{14, 15}$$

The description of $y^*(x, \lambda)$ can then be obtained in terms of the amplitude Y_m and phase angle θ_m. Observe that the nth root of equation (11) is given by the root of the equation

$$\lambda_p l_p + \theta_p = n\pi. \tag{16}$$

Thus the eigenvalues of equations (8) and (9) can be obtained by solving this equation. Once the eigenvalues are determined, equations (15) and (12) lead to the determination of the eigenfunctions. This procedure for finding the eigensolutions closely follows the formulations presented, for example, by Borland [17] and Bishop and Johnson [18].

The piecewise approximation to $\rho(x)$ and $AE(x)$ employed in the method described above is distinctly different from a finite element discretization. It may be recalled that a finite element approximation involving p elements essentially leads to estimates for the first $2p$ natural frequencies, with only the first few of these estimates being reliable. On the other hand, the procedure described in this section leads, in principle, to the entire spectrum of eigenvalues. In addition, for a rod with piecewise uniform properties the accuracy of the solutions obtained is controlled solely by the accuracy with which the root searching is performed in the solution of equation (16). This accuracy is independent of mode count and can be effectively controlled. Another significant feature of the present approach is that when $\rho(x)$ and $AE(x)$ are modelled as random processes, the probability density function of the eigensolutions can be characterized in terms of the phase angle and amplitude co-ordinates [19, 20].

Finally, for the special case of non-uniform rods in which mass and stiffness are related to each other through the relation

$$\rho_m AE_m = \text{constant}, \tag{17}$$

it follows from equations (14) and (15) that

$$\theta_{m+1} = \lambda_m l_m + \theta_m = \theta_0 + \sum_{k=1}^{m} \lambda_k l_k \qquad \text{and} \qquad Y_{m+1}/Y_m = 1. \tag{18, 19}$$

Upon noting that $\theta_0 = 0$ for rod fixed at $x = 0$, it can be easily shown that

$$\theta_p = \sum_{m=1}^{p-1} \lambda_m l_m. \tag{20}$$

Thus the characteristic equation for the eigenvalues becomes

$$\lambda_p l_p + \sum_{m=1}^{p-1} \rho_m l_m = n\pi. \tag{21}$$

This equation can further be simplified to give the nth natural frequency as

$$\omega_n = n\pi / \sum_{m=1}^{p} \rho_m l_m \tag{22}$$

and the nth mode shape in the mth subsection as

$$y_{nm}(x_m) = \sin\left[n\pi \left\{ \sum_{k=1}^{m-1} \rho_k l_k + \rho_m x_m \right\} \Big/ \sum_{k=1}^{p} \rho_k l_k \right], \qquad 0 < x_m < l_m. \tag{23}$$

These results are, in fact, the discrete analogues of the special case studied earlier by the present authors [13]. As demonstrated in the reference, they form a starting point in the analytical determination of the PDF of the eigensolutions, the Green function and the input power receptance functions of a vibrating rod. These analytical results, being exact in nature, serve as a benchmark against which alternative solution procedures can be validated. A discussion of this aspect is presented next.

6. VALIDATION OF COMPUTER PROGRAM

A Monte Carlo simulation program to calculate the statistics of the input power and coupling power receptance functions, equations (1)–(4), has been developed based on the formulations presented in sections 2 and 3. Before this program can be used with confidence, it is desirable to verify that it leads to correct solutions when run for any specific cases for which exact analytical results are available. However, to the best of the authors' knowledge there appear to be no exact solutions available for the PDF of the power flow transmission characteristics for the coupled rod configurations being studied here. On the other hand, the PDF of the dynamical characteristics of a special case of a single axially vibrating stochastic rod has recently been studied by the present authors [13]. These results may be used as benchmarks to validate the computer program developed.

Consider the axial vibration of a fixed–fixed rod in which $\rho(x)$ and $AE(x)$ vary randomly along the length of the rod. Let ρ and AE be modelled as

$$\rho(x) = \rho_0[1 + \varepsilon f(x)], \qquad AE(x) = AE_0[1 + \gamma g(x)]. \tag{24, 25}$$

Here $f(x)$ and $g(x)$ are jointly stationary random processes with zero mean and unit standard deviation. ρ_0, AE_0, ε and γ are deterministic constants. It has been shown in reference [13] that when $\rho(x)$ and $AE(x)$ are such that

$$[1 + \varepsilon f(x)][1 + \gamma g(x)] = 1 \tag{26}$$

the PDF of the eigenvalues and the Green function can be analytically determined. Furthermore, it has also been shown that the PDF of the input power receptance function for the case when the rod is driven at a point by a harmonic excitation is obtainable. In the calculations presented in reference [13] the mass process $f(x)$ is taken to be of Gaussian distribution with an autocovariance function of the form

$$R_f(x_1, x_2) = \exp[-\alpha|x_1 - x_2|]. \tag{27}$$

In Figure 2 is shown the comparison between the analytical and simulated results for the PDF of the input receptance function for the cases of a point harmonic force acting at $(x/L) = 0{\cdot}2$ with frequency $\omega = 4000$ rad/s. The simulated distribution function is estimated by using a sample size of 5000. A Kolmogorov–Smirnov goodness of fit test [21] has also been performed to verify whether the simulated result agrees with the theoretical result. The 95% confidence bands has also been marked on Figure 2. It is observed that at 5% significance level the simulated result can be taken to be distributed as per the theoretical model.

By using the procedures described in the reference it is also possible to determine analytically the PDF of the input receptance function for uniform rods in which the mass per unit length is modelled as a random variable. For the purpose of illustration, consider a rod the mass per unit length of which is modelled as a Gaussian random variable with mean 4·156 kg/m and standard deviation 15% of the mean. Let $L = 5{\cdot}182$ m, $AE = 0{\cdot}1785$ MN and $c = 80\,s^{-1}$. The theoretical result for the PDF of the input receptance function when the rod is driven by point harmonic excitation at $(x/L) = 0{\cdot}2$ is compared with the corresponding digitally simulated result in Figure 3. Results of the Kolmogorov–Smirnov goodness of fit test are also shown in these figures. Again, it is observed that, at the 5% significance level, the simulated result can be taken as drawn from a population having the theoretical PDF.

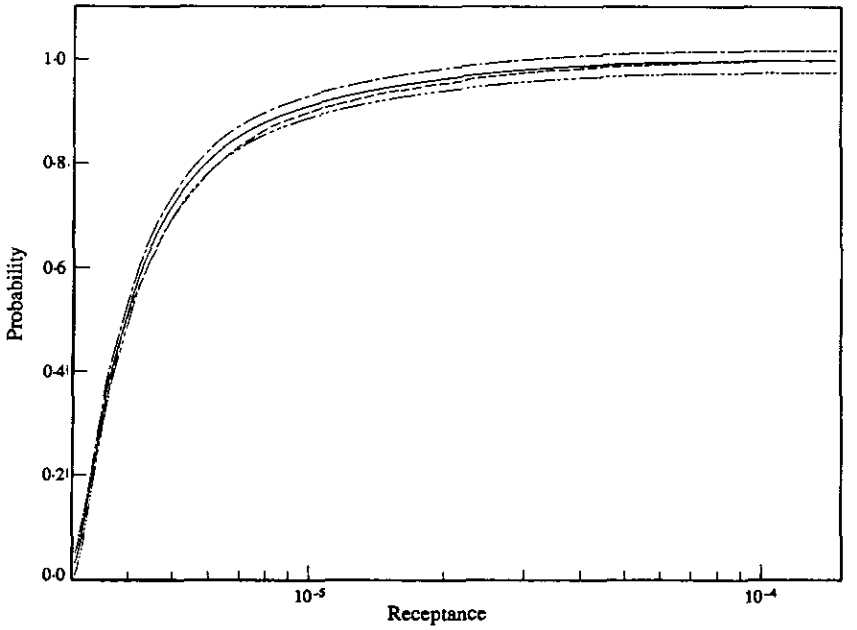

Figure 2. Theoretical and simulated input receptance probability distribution functions, $F[H_{11}(\omega)]$; point forcing, special rod, $\omega = 4000$ rad/s, $b_1 = 0{\cdot}2L$. ——, Theory; - - - -, simulation; — — —, +5%; — · — · —, −5%.

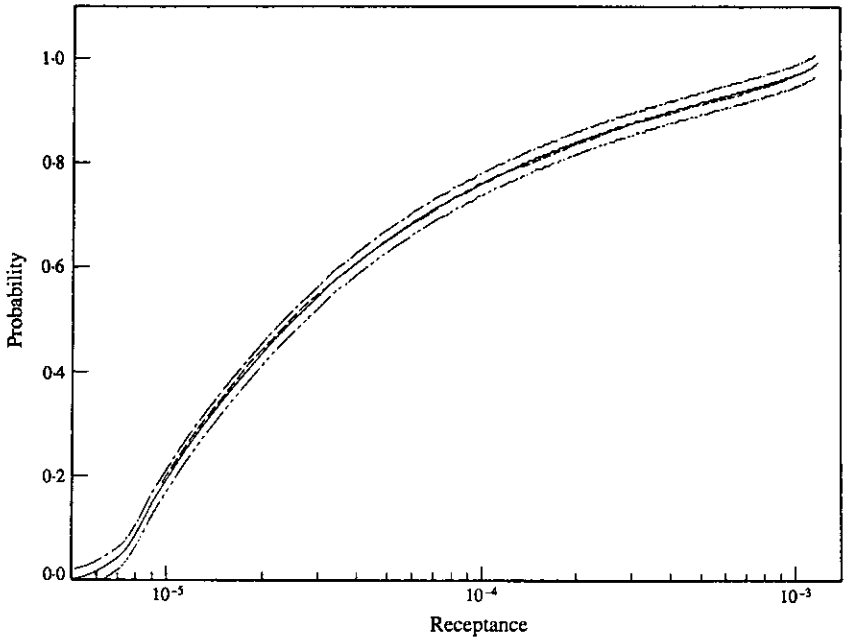

Figure 3. Theoretical and simulated input receptance probability distribution functions, $F[H_{11}(\omega)]$; point forcing, uniform rod, $\omega = 4000$ rad/s, $b_1 = 0{\cdot}2L$; key as per Figure 2.

The agreement between the theoretical and simulated results observed in Figures 2 and 3 support the use of the simulation program to study problems for which no alternative solutions are available. It must, however, be noted that it has been possible to carry out these checks only for simulation results on the behaviour of single rods. It is clearly desirable to perform such checks on the behaviour of coupled rod systems and also for individual rods when the constraints on variability of mass and stiffness are relaxed. As noted already, no analytical solutions to these problems seem to be currently available.

7. STOCHASTIC MODELS

As has already been noted, there are basically two different ways in which a stochastic model can be constructed for the *physical* properties of individual subsystems. In order of increasing complexity, the first is to model the system parameters as random variables. This means that individual realizations of the system have uniform characteristics and are reasonably well behaved. Thus, for instance, if the quantities $\rho(x)$ and $AE(x)$ are taken to be independent of x and are modelled as random variables, the eigenfunctions remain deterministic. Although the natural frequencies become random variables, distinct natural frequencies still remain linearly dependent on each other. In the context of SEA, this randomization scheme is clearly weak in character. The second and more elaborate scheme is to take the properties of the rods to be random functions of the spatial co-ordinates. Thus, $\rho(x)$ and $AE(x)$ are modelled as random processes. In this case both the natural frequencies and mode shapes become random in nature, and can be expected to show reasonably complex behaviour consistent with the conceptual framework of SEA. In using this model, further decisions have to be made regarding the spectral content and probability distribution of the spatial variations.

TABLE 1

Models for stochastic variability in rod properties

Model number	Quantity treated as random	Parameter values		Figure numbers	Details of model
		ε	α		
1	ρ	0·15 0·05	n/a n/a	8–11, 22 12–15, 22–24	$\rho = \rho_0[1 + \varepsilon u]$ u Gaussian random variable with zero mean and unit standard deviation
2	$\rho(x)$	0·25 0·1	9·5 1·3	16, 23 17, 24	$\rho(x) = \rho_0[1 + \varepsilon u(x)]$ $u(x)$ stationary Gaussian random process with zero mean and autocorrelation function $R_u(x_1, x_2) = \exp[-\alpha\|x_1 - x_2\|]$
3	$\rho(x)$	0·177 0·07	4·25 0·65	18, 23 19, 24	$\rho(x) = \rho_0\{1 + \varepsilon[u^2(x) - 1·0]\}$ $u(x)$ as per model 2
4	$AE(x)$	0·25	9·5	20, 23	$AE(x) = AE_0[1 + \varepsilon u(x)]$ $u(x)$ as per model 2
5	$d(x)$ (diameter)	0·25	9·5	21, 23	$d(x) = d_0[1 + \varepsilon u(x)]$ $u(x)$ as per model 2

The role of different stochastic modelling procedures on the probabilistic nature of the power transmission is not obvious at the outset. With a view to gaining insights into this problem, the present study has considered various different randomization schemes for modelling the subsystems. A summary of the models investigated is given in Table 1. As can be seen from the table, both Gaussian and non-Gaussian models have been considered. In this context it must be noted that the use of Gaussian models for positive quantities such as mass, stiffness or diameter is, strictly speaking, inadmissible. However, if the standard deviation of the random variations are restricted to less than 30% of the mean values, the error in the Gaussian approximation is negligibly small. This means that the parameter ε in models 1, 2, 4 and 5 of Table 1 is restricted to take values less than 0·3. In the case of models involving random processes, additional restrictions need to be imposed. Thus, for example, when $\rho(x)$ is modelled as a Guassian random process, if the standard deviation of the *total mass* of the rod is to be restricted to be less than 30% of the mean, one obtains

$$\frac{\sigma_T}{\rho_0 L} = \frac{\varepsilon}{L}\sqrt{\left[\int_0^L \int_0^L R_u(x_1, x_2)\,dx_1\,dx_2\right]} < 0·3. \tag{28}$$

Notice that this constraint involves not only ε but also the parameters in the autocovariance function of $\rho(x)$. In the studies described here, the autocovariance of the stochastic perturbation $u(x)$ for all the random process models shown in Table 1 is assumed to be of the form

$$R_u(x_1, x_2) = \exp[-\alpha|x_1 - x_2|]. \tag{29}$$

It must also be noted that the models described in Table 1 refer to the properties of a single rod. In the study of coupled rod systems, the properties of the two distinct rods are taken to be similar but statistically independent of each other.

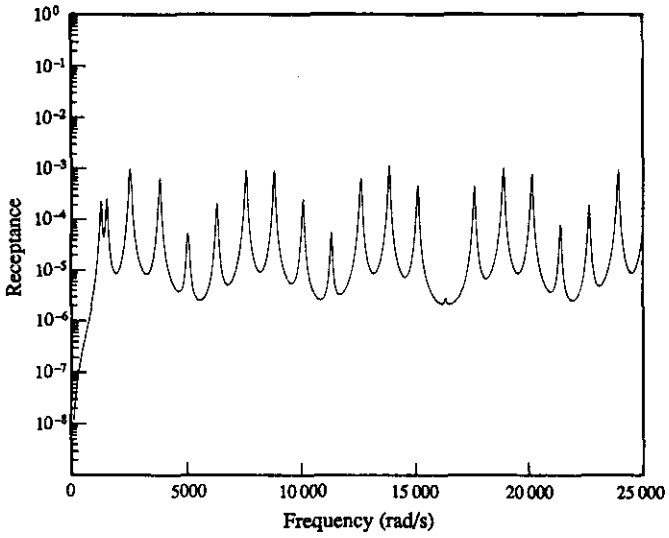

Figure 4. Deterministic input receptance function, $H_{11}(\omega)$; point forcing.

8. NUMERICAL RESULTS

The moments and PDFs of the functions $H_{11}(\omega)$ and $H_{12}(\omega)$ for both point harmonic forcing and rain on the roof type of distributed forcing have been estimated for different ensembles of coupled rod systems generated as per the models described in Table 1. These simulations are organized in such a way that the results for the different models can be directly compared with each other. Of course, for each model in the table four figures may be produced (i.e., $H_{11}(\omega)$ and $H_{12}(\omega)$ for both forcing models); here, for the sake of brevity, all four are given only for model 1 with attention being focused on just $H_{12}(\omega)$, with point forcing for the remainder. The mean values of the system properties are held fixed at $\rho_0 = 4{\cdot}156\,\text{kg/m}$, $L = 5{\cdot}182\,\text{m}$, $AE_0 = 0{\cdot}1786\,\text{MN}$ and $c = 80\,\text{s}^{-1}$. The coupling spring constant is taken to be $k_c = 0{\cdot}5 \times 10^7\,\text{N/m}$ and the points of coupling fixed at

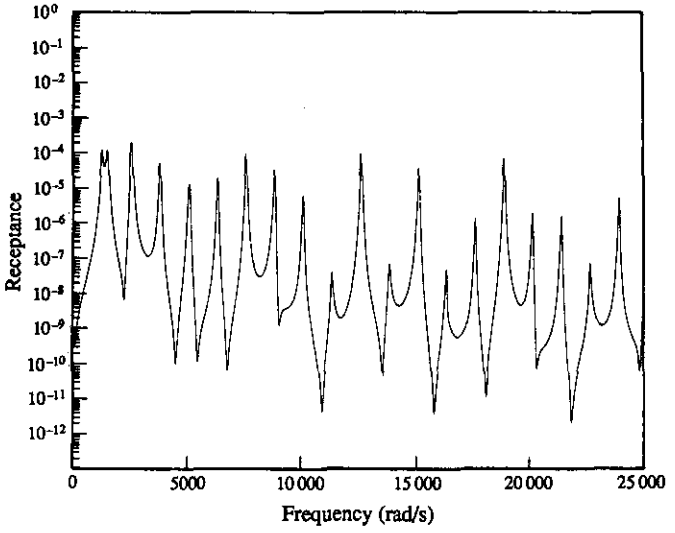

Figure 5. Deterministic cross-receptance function, $H_{12}(\omega)$; point forcing.

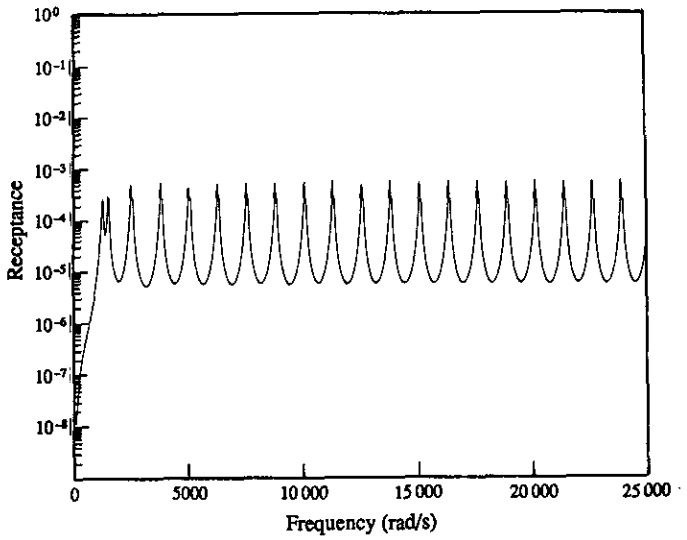

Figure 6. Deterministic input receptance function, $H_{11}(\omega)$; rain on the roof forcing.

$a_1 = 2{\cdot}3$ m ($0{\cdot}44L$) and $a_2 = 3{\cdot}3$ m ($0{\cdot}64L$). The forces are assumed to act on only the first subsystem, with the second subsystem remaining externally unforced. For point forcing the point of application is taken to be $b_1 = 1{\cdot}192$ m ($0{\cdot}23L$) and the driving frequency range of interest is taken to be 100–25 000 rad/s. The infinite summations appearing in equations (1)–(4) are carried out over modes occurring in a frequency band width of 32 000 rad/s centred at the driving frequency ω. When spatial variations in properties are used, the rods are discretized into 20 piecewise uniform elements of equal length. The variations of the various statistics of the receptances have been computed as functions of driving frequency ω with response statistics being estimated by using an ensemble sample size of 2500. For reference, plots of $H_{11}(\omega)$ and $H_{12}(\omega)$ for the case of the deterministic system ($\varepsilon = 0$)

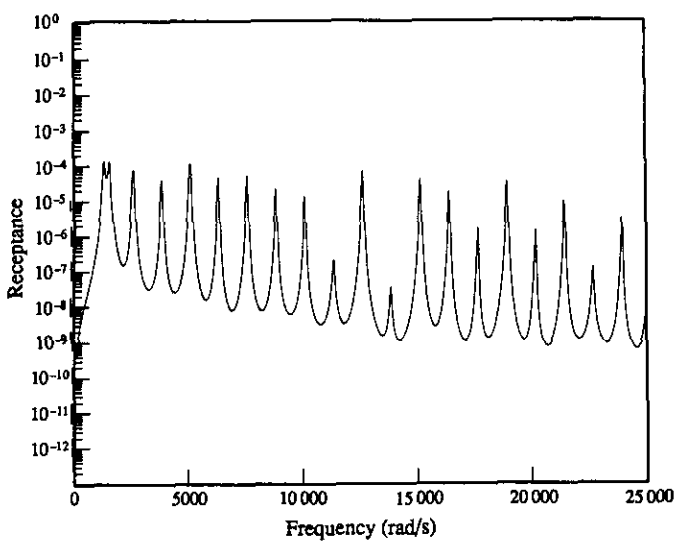

Figure 7. Deterministic cross-receptance function, $H_{12}(\omega)$; rain on the roof forcing.

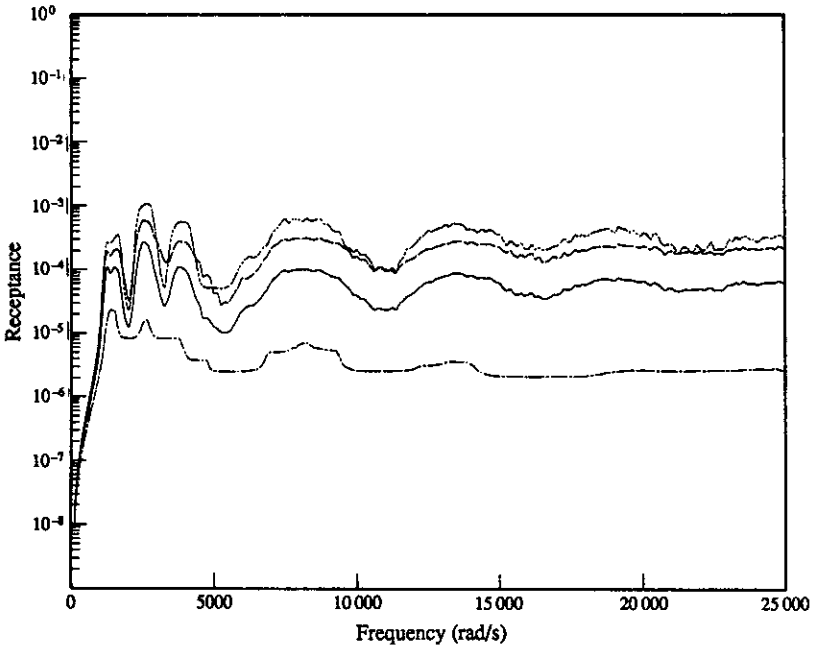

Figure 8. Input receptance statistics, $E[H_{11}(\omega)]$, etc.; point forcing, model 1, $\varepsilon = 0{\cdot}15$, $b_1 = 0{\cdot}23L$. ——, Mean; - - - -, mean plus one standard deviation; — · —, 5% probability level; — - - - —, 95% probability level.

excited by these two types of forces are given in Figures 4–7. It may be noted that for a fixed–fixed rod with these properties, the nth natural frequency is given by $\omega_n = 1256n$ rad/s and, consequently the modal overlap factor is 0·06.

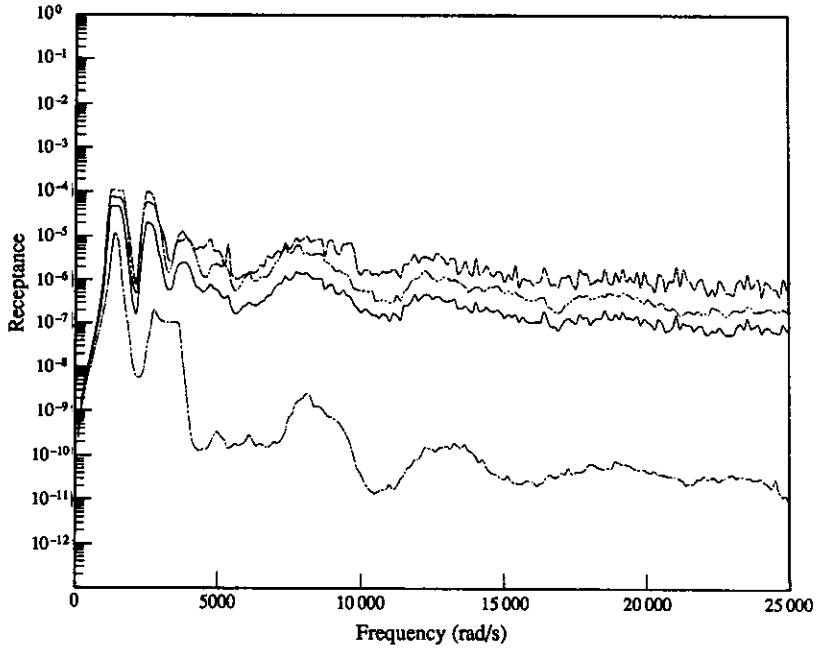

Figure 9. Cross-receptance statistics, $E[H_{12}(\omega)]$, etc.; point forcing, model 1, $\varepsilon = 0{\cdot}15$, $b_1 = 0{\cdot}23L$; key as per Figure 8.

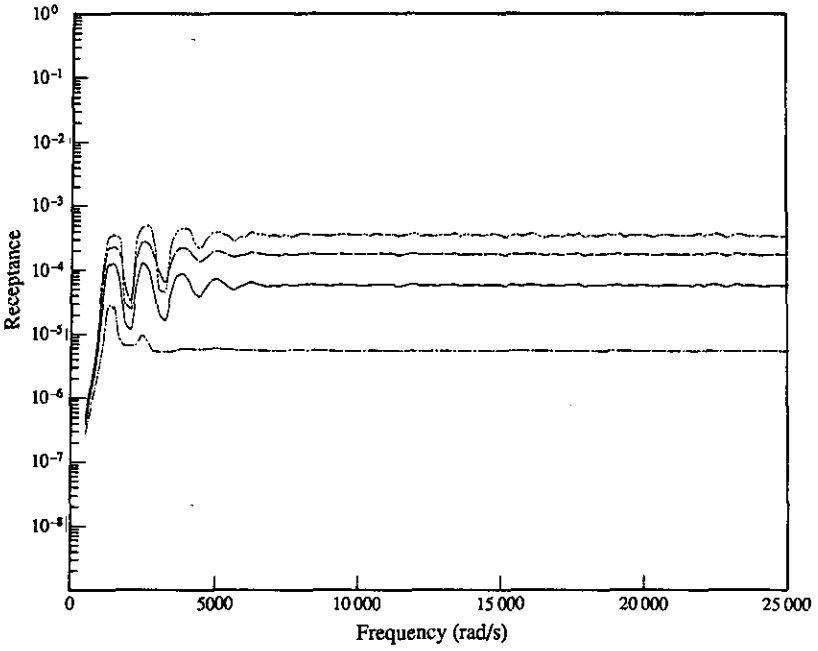

Figure 10. Input receptance statistics, $E[H_{11}(\omega)]$, etc.; rain on the roof forcing, model 1, $\varepsilon = 0{\cdot}15$; key as per Figure 8.

The effect of varying just the overall mass, using uniform rods, that is, model 1, is illustrated in Figures 8–15, with the randomness parameter ε being held at 0·15 for the first four figures and reduced to 0·05 for the remainder. When the mass density is also allowed

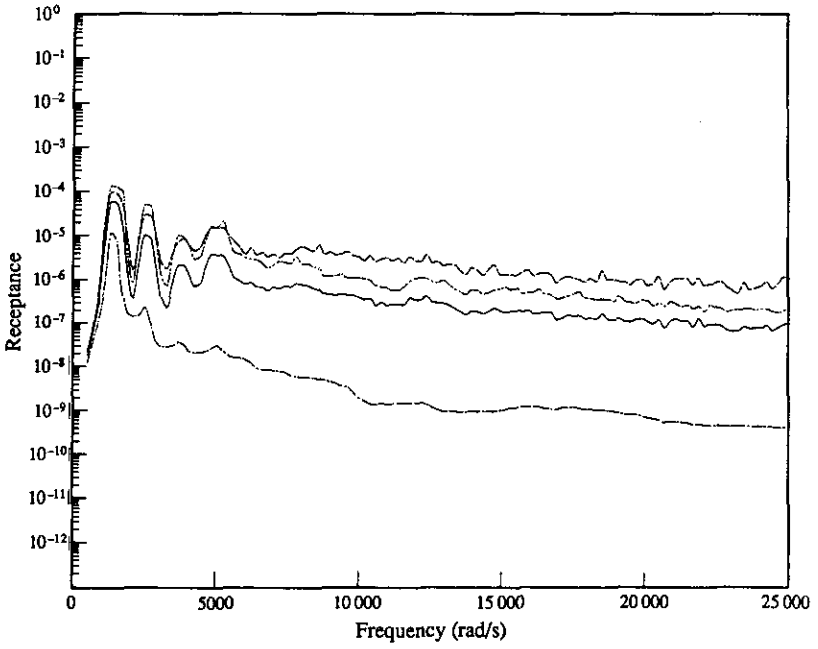

Figure 11. Cross-receptance statistics, $E[H_{12}(\omega)]$, etc.; rain on the roof forcing, model 1, $\varepsilon = 0{\cdot}15$; key as per Figure 8.

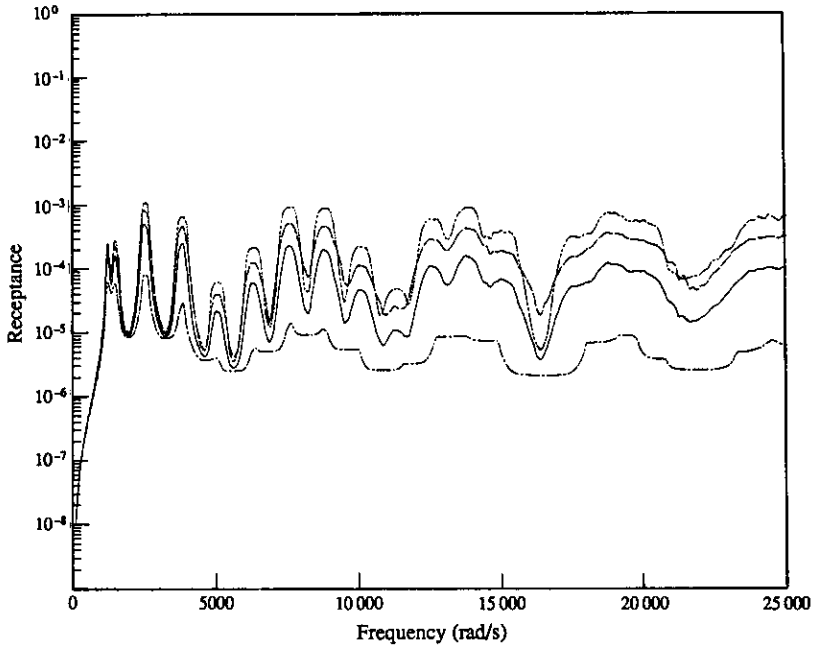

Figure 12. Input receptance statistics, $E[H_{11}(\omega)]$, etc.; point forcing, model 1, $\varepsilon = 0{\cdot}05$, $b_1 = 0{\cdot}23L$; key as per Figure 8.

to vary along the length of the rod, model 2, the additional parameter α in the autocovariance is used to characterize these spatial variations. In such cases the total mass depends on both ε and α and these are chosen such that the total masses have the

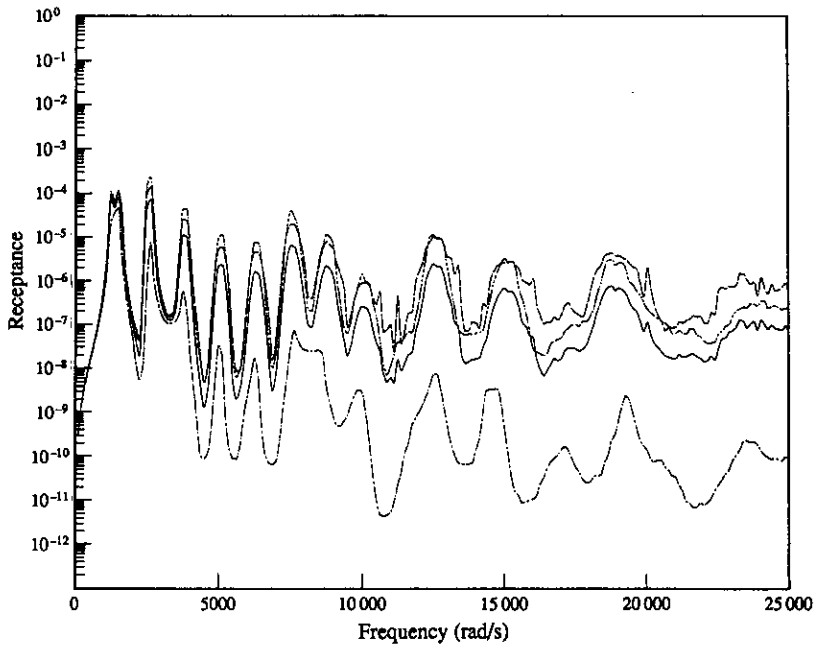

Figure 13. Cross-receptance statistics, $E[H_{12}(\omega)]$, etc.; point forcing, model 1, $\varepsilon = 0{\cdot}05$, $b_1 = 0{\cdot}23L$; key as per Figure 8.

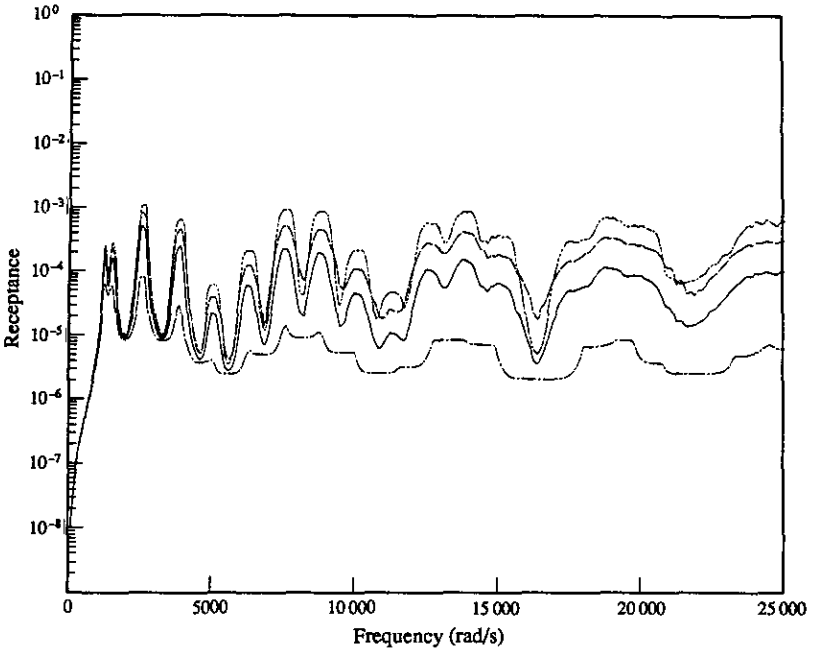

Figure 14. Input receptance statistics, $E[H_{11}(\omega)]$, etc.; rain on the roof forcing, model 1, $\varepsilon = 0{\cdot}05$; key as per Figure 8.

same Gaussian distribution as for the case of $\varepsilon = 0{\cdot}05$ with model 1 (i.e., Figures 12–15). The effects of broad- and narrow-band spatial variations for this model are illustrated in Figures 16 and 17, respectively, which are for $\varepsilon = 0{\cdot}25$ with $\alpha = 9{\cdot}5$ and $\varepsilon = 0{\cdot}1$ with $\alpha = 1{\cdot}3$.

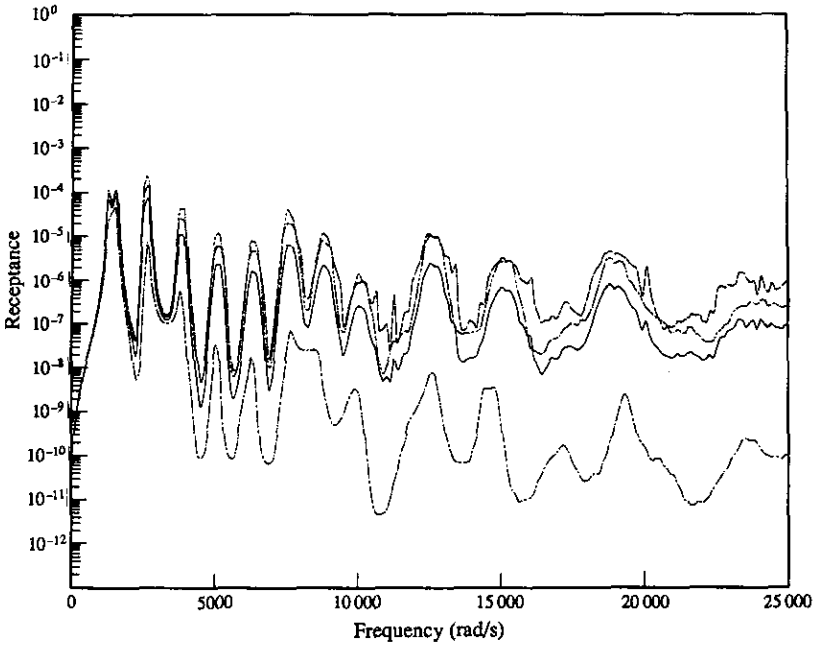

Figure 15. Cross-receptance statistics, $E[H_{12}(\omega)]$, etc.; rain on the roof forcing, model 1, $\varepsilon = 0{\cdot}05$; key as per Figure 8.

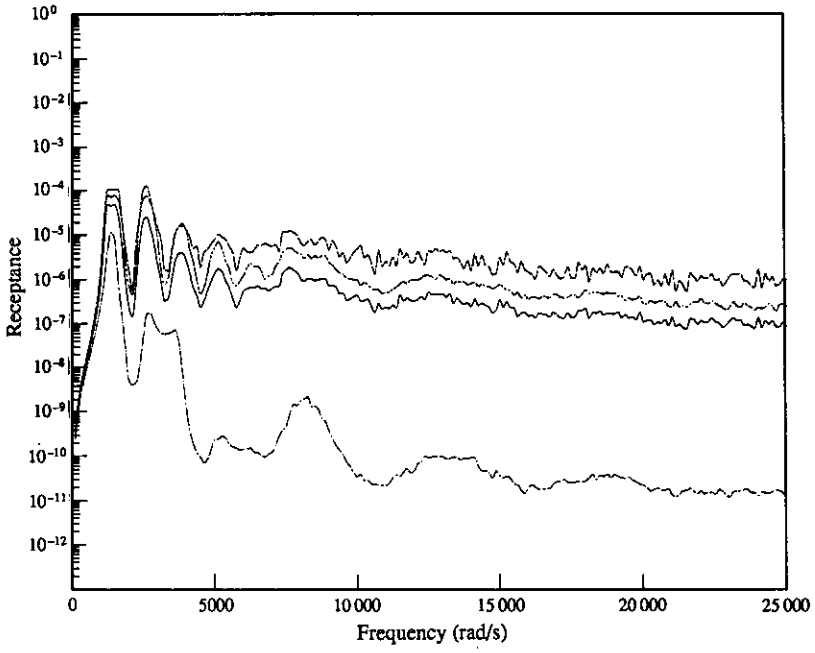

Figure 16. Cross-receptance statistics, $E[H_{12}(\omega)]$, etc.; point forcing, model 2, $\varepsilon = 0{\cdot}25$, $\alpha = 9{\cdot}5$, $b_1 = 0{\cdot}23L$; key as per Figure 8.

The effect of assuming $\rho(x)$ to be a non-Gaussian random process (model 3) is shown in Figures 18 and 19, again for broad- and narrow-band spatial variations. Clearly, it is not possible to establish equivalence in terms of PDF

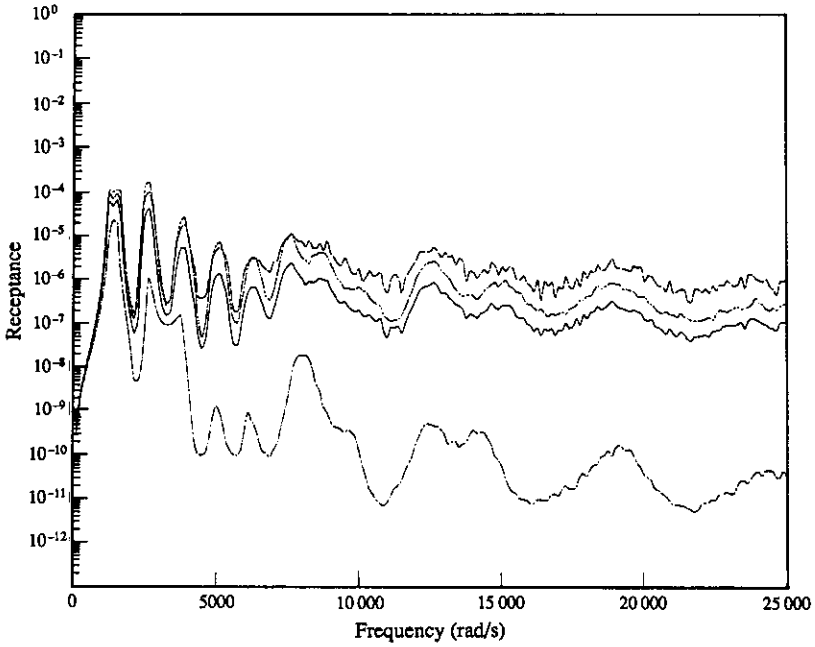

Figure 17. Cross-receptance statistics, $E[H_{12}(\omega)]$, etc.; point forcing, model 2, $\varepsilon = 0{\cdot}1$, $\alpha = 1{\cdot}3$, $b_1 = 0{\cdot}23L$; key as per Figure 8.

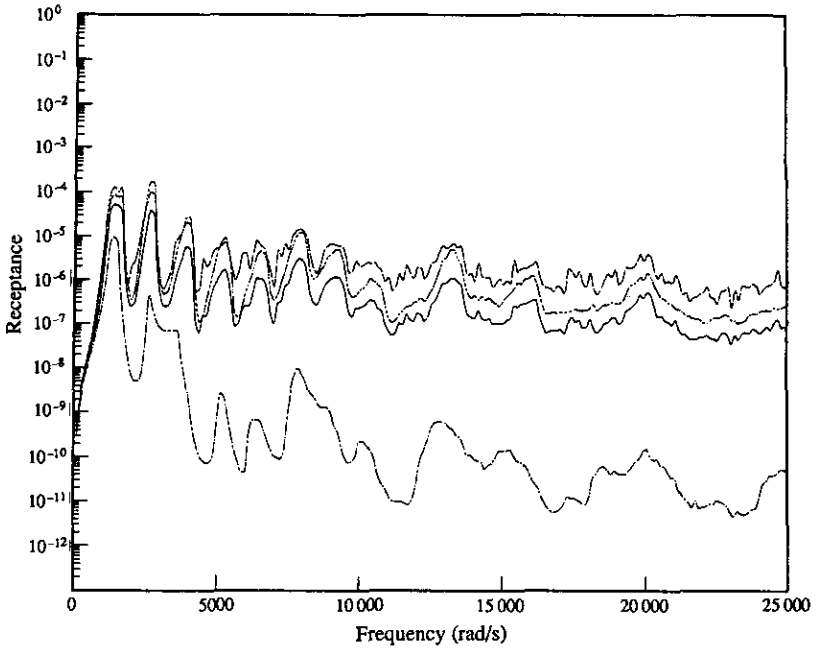

Figure 18. Cross-receptance statistics, $\mathrm{E}[H_{12}(\omega)]$, etc.; point forcing, model 3, $\varepsilon = 0{\cdot}177$, $\alpha = 4{\cdot}25$, $b_1 = 0{\cdot}23L$; key as per Figure 8.

for total masses between the results for this model and those for the Gaussian processes of models 1 and 2. It is still possible, however, to establish equivalence of the mean an autocovariance of $\rho(x)$ between models 2 and 3,

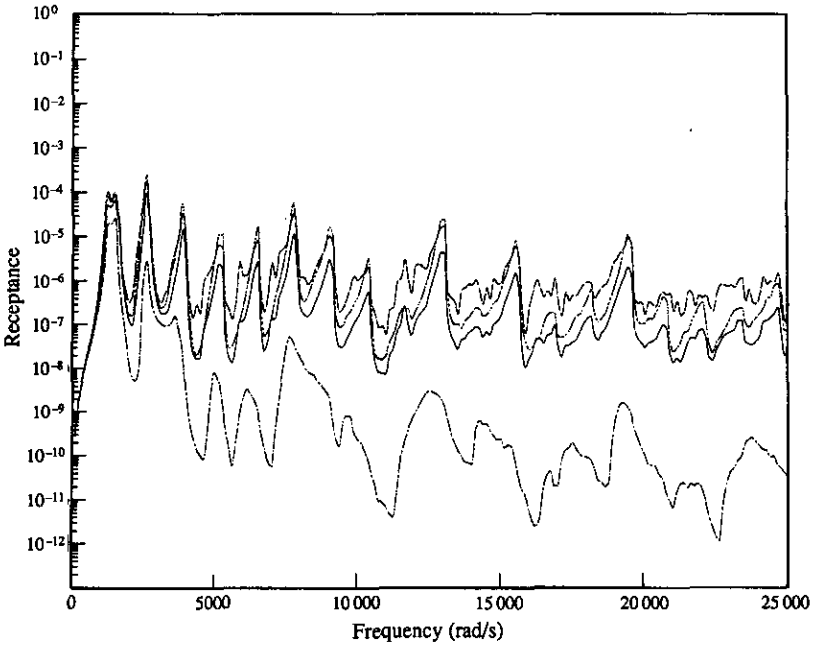

Figure 19. Cross-receptance statistics, $\mathrm{E}[H_{12}(\omega)]$, etc.; point forcing, model 3, $\varepsilon = 0{\cdot}07$, $\alpha = 0{\cdot}65$, $b_1 = 0{\cdot}23L$; key as per Figure 8.

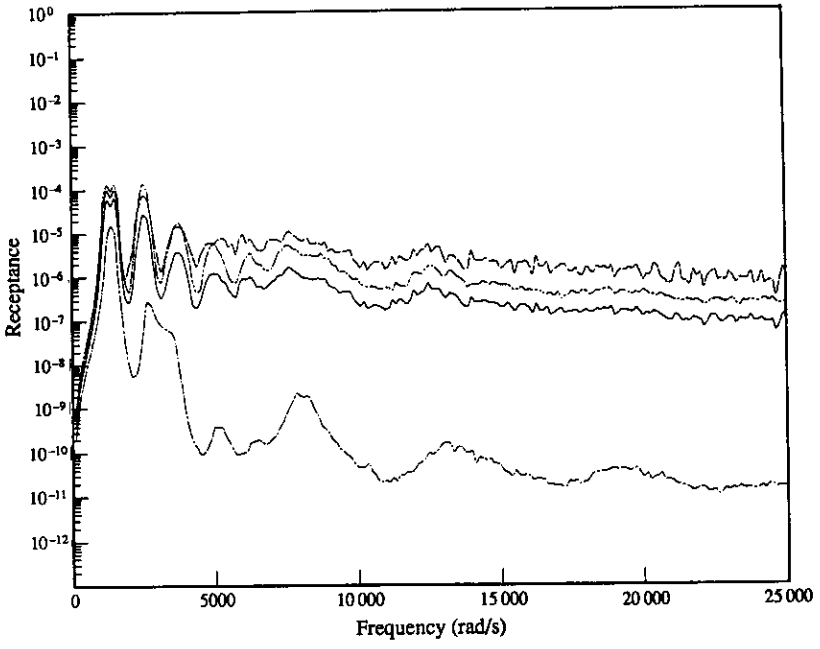

Figure 20. Cross-receptance statistics, $E[H_{12}(\omega)]$, etc.; point forcing, model 4, $\varepsilon = 0{\cdot}25$, $\alpha = 9{\cdot}5$, $b_1 = 0{\cdot}23L$; key as per Figure 8.

and this has been achieved here by using $\varepsilon = 0{\cdot}177$ with $\alpha = 4{\cdot}25$ and $\varepsilon = 0{\cdot}07$ with $\alpha = 0{\cdot}65$ in Figures 18 and 19, being equivalent to Figures 16 and 17, respectively.

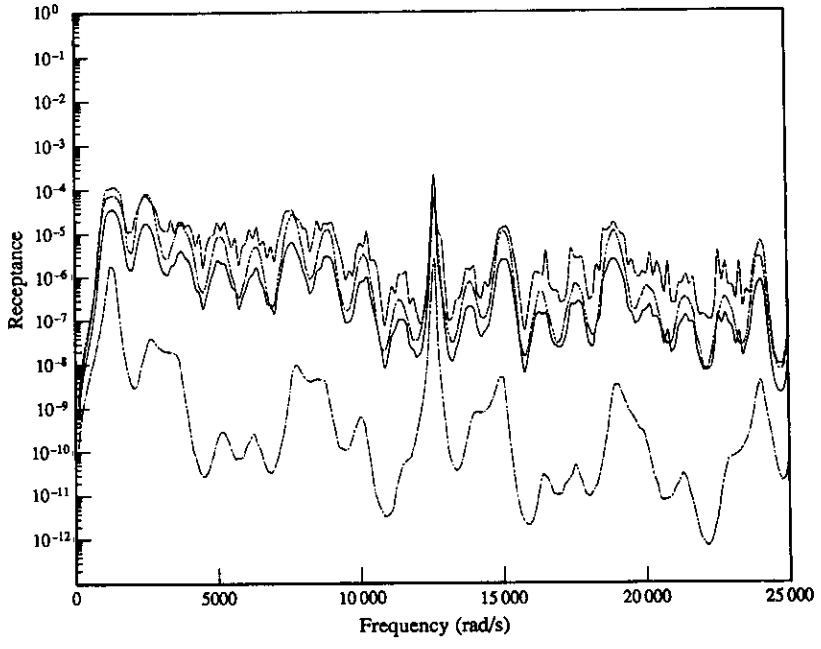

Figure 21. Cross-receptance statistics, $E[H_{12}(\omega)]$, etc.; point forcing, model 5, $\varepsilon = 0{\cdot}25$, $\alpha = 9{\cdot}5$, $b_1 = 0{\cdot}23L$; key as per Figure 8.

The case in which the stiffness $AE(x)$ is modelled as a Gaussina random process instead of the mass, model 4, is shown in Figure 20 for $\varepsilon = 0{\cdot}25$ and $\alpha = 9{\cdot}5$; cf. Figure 16 for model 2. Finally, the results for the case when the subsystems are modelled as rods with circular cross-sections with the diameter varying as a Gaussian random process (model 5) for $\varepsilon = 0{\cdot}25$ and $\alpha = 9{\cdot}5$ are presented in Figure 21. In view of the fact that the mass per unit length and stiffness are functions of square of the diameter, the models for ρ and AE in this case are given by

$$\rho(x) = \rho_0[1 + \varepsilon u(x)]^2, \qquad AE(x) = AE_0[1 + \varepsilon u(x)]^2. \tag{31}$$

In this case therefore, $\rho(x)$ and $AE(x)$ not only have non-Gaussian character but are also linearly dependent on each other.

To summarize these results, in Figures 4–15 comparisons are allowed of the input and cross-power receptances for both point and rain on the roof forcing, in each case with results for deterministic calculations plus two levels of randomness. In Figures 5, 13, 16, 18, 20 and 21, the cross-power receptances are compared for the deterministic case plus the five randomization schemes adopted, all with point forcing, the smaller degree of randomization used in Figures 11–15 and broadbanded spatial variations. Finally, in Figures 5, 13, 17 and 19 the deterministic case plus the first three randomization schemes are contrasted with a reduced spatial bandwidth, again for point forcing and showing the cross-power receptances. These three comparisons are further aided by studying Figures 22–24, respectively, which show the probability distribution functions of the cross-power receptances for the various models used, at a fixed frequency of 10 000 rad/s. Notice that the horizontal axes have logarithmic

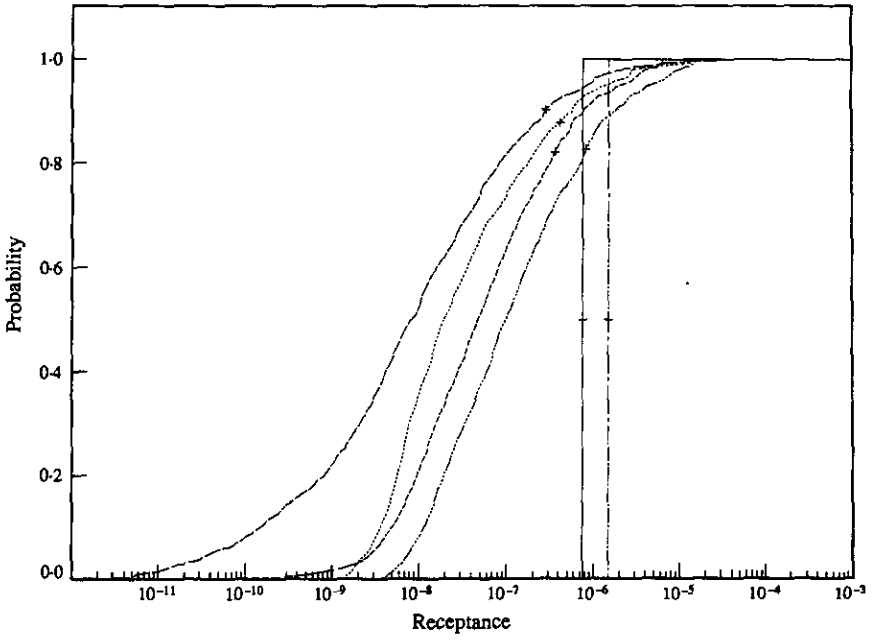

Figure 22. Cross-receptance probability distribution functions, $F[H_{12}(\omega)]$; point and rain on the roof forcing, model 1, $\varepsilon = 0{\cdot}0$, $0{\cdot}15$, and $0{\cdot}05$, $\omega = 10\,000$ rad/s, $b_1 = 0{\cdot}23L$. ——, Point forcing, deterministic case, $\varepsilon = 0{\cdot}0$; — — —, point forcing, $\varepsilon = 0{\cdot}15$; – – –, point forcing, $\varepsilon = 0{\cdot}05$; — · —, rain on the roof forcing, deterministic case, $\varepsilon = 0{\cdot}0$; · · ·, rain on the roof forcing, $\varepsilon = 0{\cdot}15$; — · · · —, rain on the roof forcing, $\varepsilon = 0{\cdot}05$.

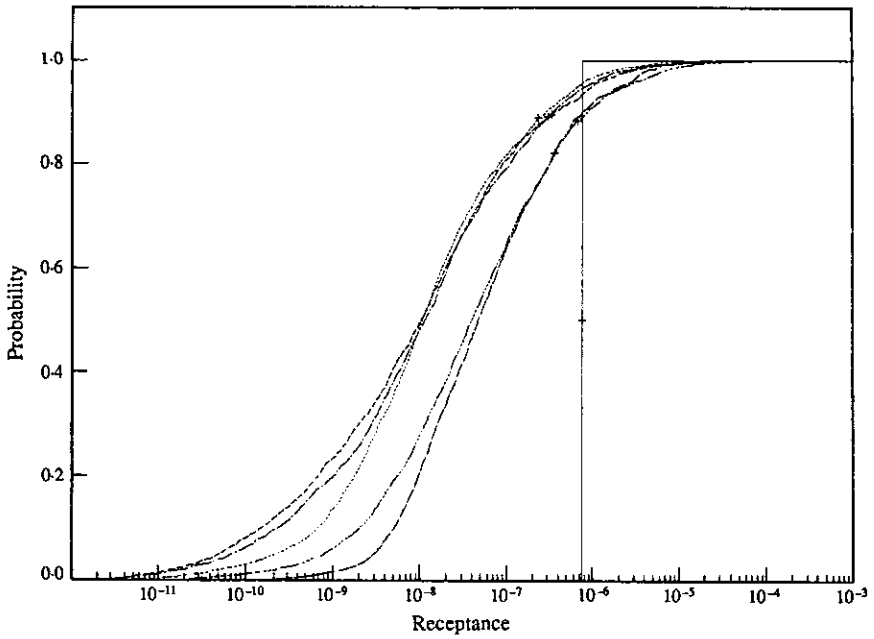

Figure 23. Cross-receptance probability distribution functions, $F[H_{12}(\omega)]$; point forcing, models 1–5, ε, α broadbanded (see Table 1), $\omega = 10\,000$ rad/s, $b_1 = 0{\cdot}023L$. ——, Deterministic case; — — —, model 1; – – –, model 2; - - -, model 3; — · —, model 4; — - - - —, model 5.

scales in these plots, since the earlier figures are also plotted on a logarithmic basis. Also, the mean values of the receptances at this frequency are marked with a "+" on the figures.

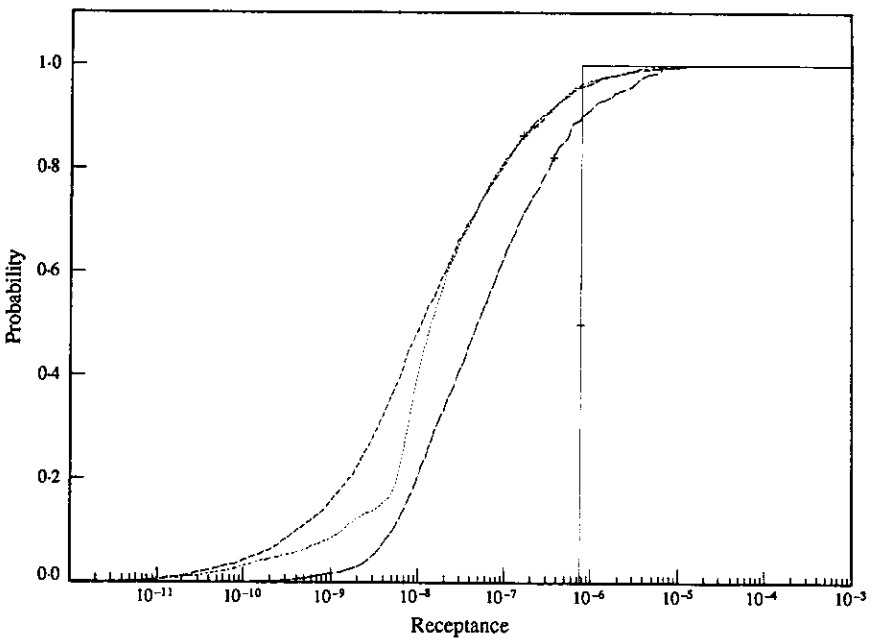

Figure 24. Cross-receptance probability distribution functions, $F[H_{12}(\omega)]$; point forcing, models 1–3, ε, α narrow banded (see Table 1), $\omega = 10\,000$ rad/s, $b_1 = 0{\cdot}23L$. ——, Deterministic case; — — —, model 1; – – –, model 2; - - -, model 3.

9. DISCUSSION

A general freature than can be observed in the majority of the cases illustrated in Figures 8–21 is that, beyond a limiting frequency ω^*, the receptance functions tend to become *stochastically* stationary. This frequency can be thought of as the cut-off frequency below which traditional SEA approximations are unlikely to hold. Several factors pertaining to excitation and the details of statistical modelling of sybsystems appear to control this limiting frequency. On the whole, it is seen that the rain on the roof type of excitation leads more quickly to steady behaviour than point forcing. Also, the function $H_{11}(\omega)$ is seen to be much more well behaved in this aspect than $H_{12}(\omega)$. The strength of randomness, and whether or not a random process or a random variable model is used, further affects ω^*. Thus, from Figures 8–11 and 12–15 it can be seen that a reduction in ε from 15% to 5% significantly increases the cut-off frequency ω^*. This is as expected, since as $\varepsilon \to 0$ the curves all tend to the deterministic results of Figures 4–7 which, of course, show no tendency towards steady behaviour, instead being dominated by the individual model peaks and troughs of the subsystems. Notice that although reducing the randomness in this way increases the cut-off frequency it reduces the measures of dispersion; this is as expected since there is no dispersion in the deterministic case. This is more clearly seen in Figure 22, which shows the probability distribution functions for the two levels of randomization adopted in model 1: the slopes of the functions increase, tending to step functions, as ε is reduced and the dispersion decreases. A similar change is noted when moving from point to rain on the roof forcing.

From Figures 13, 16 and 17, it can be noted that, at an equal level of randomness in total mass, a relatively broadbanded random process model for $\rho(x)$ results in smoother behaviour for the receptance functions. This behaviour is also seen when comparing Figures 23 and 24, where the distribution function is seen to be shallower for the broadbanded models. In consequence, the difference between the results of the random variable model, Figure 13, and random process models, Figures 16 and 17, is most significant for the case when $\rho(x)$ is broadbanded (Figure 16). This arises naturally because the mass profiles for narrow-band variations tend to be slowly varying and thus have a closer resemblance to those of the random variable model. Conversely, when $\rho(x)$ is broadbanded, it is capable of faster fluctuations and, therefore, significant differences from the random variable model.

The effect of assuming non-Gaussian distributions for $\rho(x)$, model 3, is seen in Figures 18 and 19. As has already been noted, the random perturbation $[u^2(x) - 1{\cdot}0]$ here is equivalent to the Gaussian perturbations leading to Figures 16 and 17, in the *limited* sense that the perturbations here have similar mean and autocovariance functions. A comparison between these four figures reveals significant differences in the behaviour of the receptance statistics. It is observed that a Gaussian model for $\rho(x)$ is more favourable to the steady behaviour of the statistics of $H_{12}(\omega)$ than a non-Gaussian model. However, even in this case, the broadband model of Figure 18 is found to be more favourable in this sense than the narrow-band model of Figure 19. Nonetheless, Figures 23 and 24 reveal that although the mean and measures of dispersion arising from the non-Gaussian models take longer to reach steady state, they do not necessarily show significantly greater statistical variation at any given frequency.

The results discussed thus far pertain to the modelling of $\rho(x)$ as a random quantity. Limited studies on alternative randomization schemes involving parameters other than ρ have also been carried out. Thus, in Figure 20 are shown the results for the case in which $AE(x)$ is modelled as a Gaussian random process, model 4. The perturbation $u(x)$, impressed on $AE(x)$, in this case has properties similar to the case considered in Figure 16, where $\rho(x)$ is given an identical perturbation. It is interesting to observe that

the results corresponding to these two cases show good agreement; this is also seen in Figure 23.

The role of modelling diameter as a Gaussian random process, model 5, is investigated in Figure 21. As has already been pointed out, the mass and stiffness for this model have non-Gaussian probability distributions and are linearly dependent on each other. Interestingly, in this case the receptance function statistics fail to reach a steady state. In fact, the variations in statistics, closely resemble the results for the deterministic case shown in Figure 5. The regular behaviour observed for this model possibly arises from the linear dependence existing between ρ and AE, which makes the ratio ρ/AE a deterministic quantity. The behaviour of the receptance at around 12 500 rad/s, where the function peaks and the statistical dispersion narrows, is curious. It is related to the fact that, at this frequency, mode 10 dominates the response and 20 elements have been used to discretize the spatial variations: i.e., a node tends to fall at each element boundary. However, such behaviour is not seen in the other models, and it remains unexplained for this case. Clearly, it is not amenable to an approximate analysis using traditional SEA assumptions.

As has already been noted, the mean values of $H_{12}(\omega)$ are shown in Figures 22–24 marked by a "+". These all lie at broadly the same point, which is as expected since the mean values of the subsystem properties in all the cases shown in the figures are held fixed. However, it is clear that there are very long upper tails to the functions: at some frequencies in Figures 13 and 15 for instance, the mean rises above the 95% probability level. These tails only appear on *both* sides of the mean when studying logarithmic values, as is normal in energy flow work. In such circumstances the mean lies well to one side of the probability functions, and points once again to the use of geometric averaging when studying the statistics of such flows [22]. This would, of course, imply significant changes to the generally accepted forms of SEA.

In summary, it can be said that the statistics of power receptance functions are not robust with respect to the details of the statistical models adopted for the system properties: i.e., the statistics do not always tend to steady state with increasing frequency, the rate of convergence being very susceptible to the model adopted. It is especially poor for cases with low and medium frequency ranges, small degrees of randomness, narrow-banded or non-Gaussian processes. Even where the statistical variations of $H_{11}(\omega)$ and $H_{12}(\omega)$ do reach a steady state, the measures of dispersion, namely the standard deviation and the band enclosing 5% and 95% probability levels, do not tend to reduce with increases in the driving frequency. In other words, despite the fact that there is a much greater variability in the eigensolutions at higher frequencies, the dispersion in the response at these frequencies does not reduce. This points towards significant correlations between eigensolutions in the higher frequency ranges, and also indicates the possible invalidity of arguments based on the central limit theorem in these contexts. It may also be related to the constant model densities and low modal overlap factors exhibited by the stochastic rod models used here. Finally, the probability distributions have long upper tails which cause the arithmetic mean to be a relatively poor predictor of typical response, the geometric mean being more useful in this respect.

10. EXTREME RESPONSES AND CRITICAL SYSTEMS

From a statistical ensemble of vibrating systems it is clearly of engineering interest to identify the individual members of the ensemble the responses of which depart most significantly from the mean response. Such systems can be easily identified in a

Monte Carlo simulation study. To illustrate this, consider the coupled rod excited by a point harmonic force with frequency $\omega = 10\,000$ rad/s (1·59 kHz) acting on the first rod at $b_1 = 1{\cdot}192$ m ($0{\cdot}23L$) as before. Let the individual rods be drawn for a statistical ensemble generated as per the stochastic model 2 with $\varepsilon = 0{\cdot}25$ and $\alpha = 0{\cdot}95$ with an ensemble of 10 000 systems. Based on these calculations the extreme values of the receptance and corresponding individual realizations of the system which generate them were identified. The responses were found to be $H_{12min} = 0{\cdot}128668\text{E-}12$ and $H_{12max} = 0{\cdot}166309\text{E-}03$.

For the first of these cases, the subsystem critical mass profiles, associated mode shapes in the neighbourhood of the driving frequency of $\omega = 10\,000$ rad/s (1·59 kHz) and the overall behaviour of the receptance function are shown in Figures 25–27. From a careful study of the figures, it can be discerned that neither of the two rods has a natural frequency near the driving frequency, and that the mode shapes tend to have low values at the points of coupling ($a_1 = 2{\cdot}3$ m, $a_2 = 3{\cdot}3$ m) and driving ($b_1 = 1{\cdot}192$ m). In other words, the distribution of the mass in the critical system tends to make the driving frequency an anti-resonant frequency for the system, which, in turn, pushes the response to this extreme. Similar, but reversed, trends are observed for the case of H_{12max}.

If the determination of the extreme responses and the corresponding "optimal" systems is alone of interest, then Monte Carlo simulation procedures are perhaps not the most efficient methods for solving the problem. This is because the extreme responses are essentially rare in character and hence are sensitive to the sample size used in the simulations. Alternatively, numerical optimization schemes provide efficient means with which to handle this problem. For the purpose of illustration again, consider two axially vibrating rods made up of 20 piecewise uniform sections of equal length. Let ρ_{im}, $i = 1, 2$, $m = 1, 20$, be the mass per unit length of the ith rod in the mth section. Other properties of the rod and the details of coupling are taken to be identical to the mean properties considered in section 6. Again, let this system be excited by a harmonic force with frequency $\omega = 10\,000$ rad/s acting on the first rod at $b_1 = 1{\cdot}192$ m. Let it be required to determine values of ρ_{im}, $i = 1, 2$, $m = 1, 20$, which lead, respectively, to the minimum and maximum of the function $H_{12}(\omega)$ at $\omega = 10\,000$ rad/s. It may be recalled that in the determination of "optimal" systems based on Monte Carlo simulations, the vibrating rods were constrained to belong to a statistical ensemble having prescribed properties. In the present case a similar

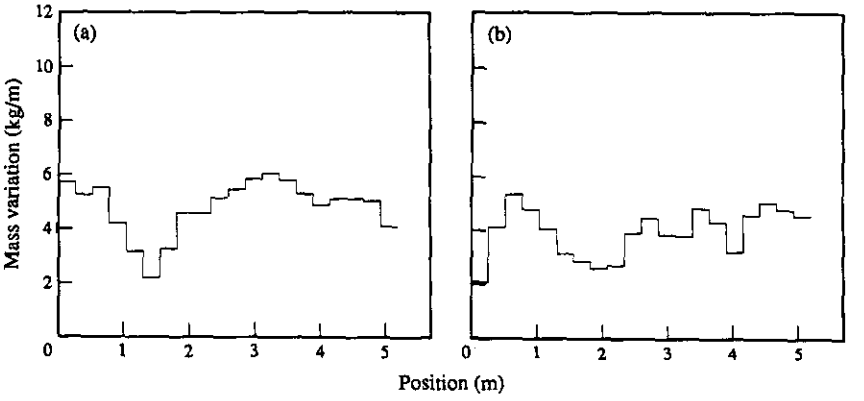

Figure 25. Mass profiles for system with minimum cross-receptance function, $H_{12min}(\omega)$; point forcing, model 2, Monte Carlo simulation, $\epsilon = 0{\cdot}25$, $\alpha = 9{\cdot}5$, $\omega = 10\,000$ rad/s, $b_1 = 0{\cdot}23L$. (a) Subsystem 1; (b) subsystem 2.

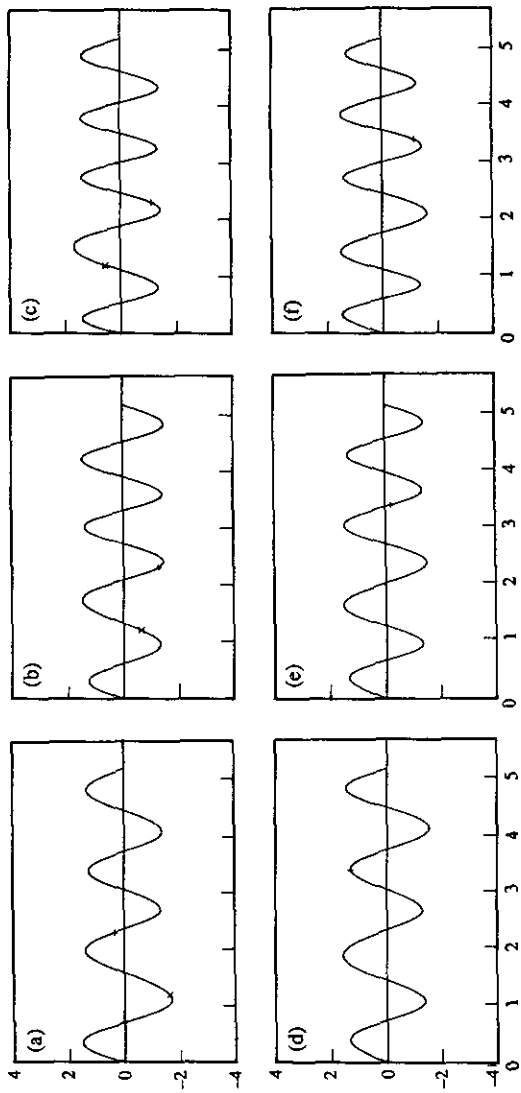

Figure 26. Mode shapes for system with minimum cross-receptance function, $H_{12min}(\omega)$ (axial variations show transverse for clarity); point forcing, model 2, Monte Carlo simulation, $\varepsilon = 0{\cdot}25$, $\alpha = 9{\cdot}5$, $\omega = 10\,000$ rad/s, $b_1 = 0{\cdot}23L$. +, Coupling point; ×, drive point. Subsystem 1: (a) mode 7, 1·301 kHz; (b) mode 8, 1·488 kHz; (c) mode 9, 1·687 kHz. Subsystem 2: (d) mode 7, 1·475 kHz; (e) mode 8, 1·638 kHz; (f) mode 9, 1·856 kHz.

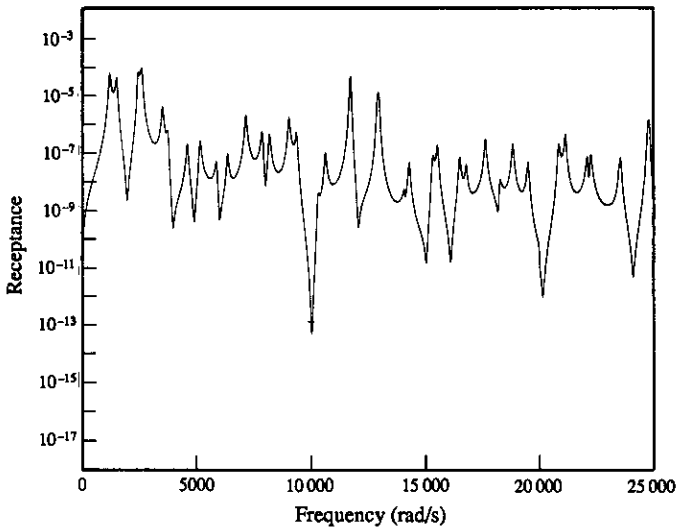

Figure 27. Deterministic cross-receptance function, $H_{12}(\omega)$, for system with minimum cross-receptance function, $H_{12min}(\omega)$; point forcing, model 2, Monte Carlo simulation, $\varepsilon = 0{\cdot}25$, $\alpha = 9{\cdot}5$, $\omega = 10\,000$ rad/s, $b_1 = 0{\cdot}23L$. +, $H_{12min}(\omega)$.

constraint also needs to be imposed on the variables ρ_{im}. This is achieved by requiring that the total mass of the individual rods, given by

$$m_i = \sum_{m=1}^{20} l_m \rho_{im}, \qquad i = 1, 2 \tag{32}$$

takes values in the range $3 < m_i < 50$ kg, $i = 1, 2$, along with the restriction that $0{\cdot}5 < \rho_{im} < 10{\cdot}0$ kg/m. Application of a genetic algorithm approach to this problem, with 50 generations of 50 members (see, for example, the paper by Goldberg [23]), leads to mass distributions that give $H_{12min} = 0{\cdot}4926790\text{E-}19$ and $H_{12max} = 0{\cdot}476113\text{E-}03$: that is, respectively, 3·82E-07% and 286·8% of the corresponding extreme results determined by using Monte Carlo simulations. Again, the details of the optimal mass profiles and the corresponding subsystem mode shapes and variations of the receptance functions for the

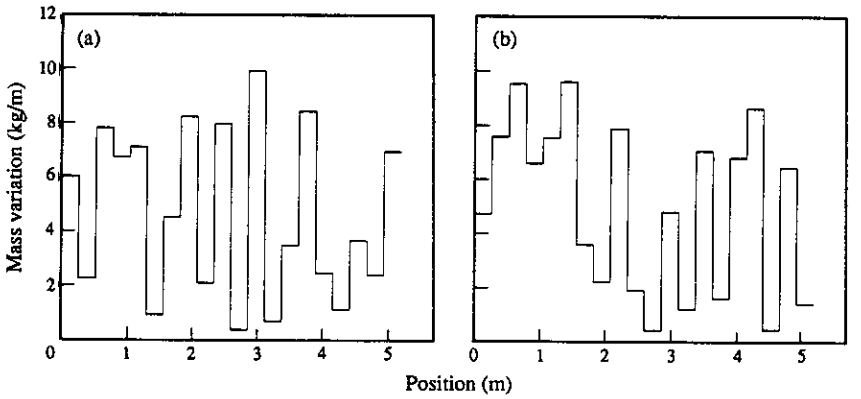

Figure 28. Mass profiles for system with minimum cross-receptance function, $H_{12min}(\omega)$; point forcing, genetic algorithm optimization, $3 < m_i < 50$ kg, $0{\cdot}5 < \rho_{im} < 10{\cdot}0$ kg/m, $\omega = 10\,000$ rad/s, $b_1 = 0{\cdot}23L$. (a) Subsystem 1; (b) subsystem 2.

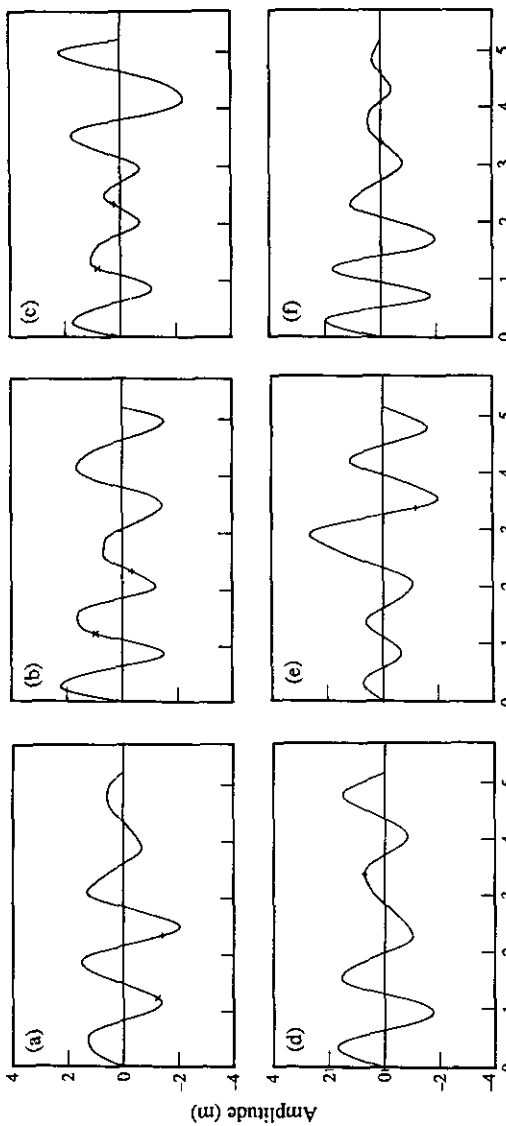

Figure 29. Mode shapes for system with minimum cross-receptance function, $H_{12min}(\omega)$ (axial variations show transverse for clarity); point forcing, genetic algorithm optimization, $3 < m_i < 50$ kg, $0{\cdot}5 < \rho_{im} < 10{\cdot}0$ kg/m, $\omega = 10\,000$ rad/s, $b_1 = 0{\cdot}23L$. +, Coupling point; × drive point. Subsystem 1: (a) mode 7, 1·270 kHz; (b) mode 8, 1·721 kHz; (c) mode 9, 1·749 kHz. Subsystem 2: (d) model 7, 1·252 kHz; (e) mode 8, 1·414 kHz; (f) mode 9, 1·645 kHz.

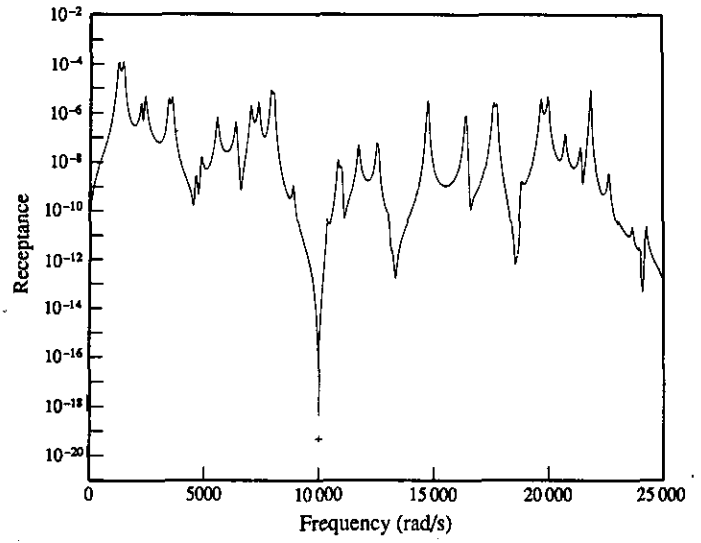

Figure 30. Deterministic cross-receptance function, $H_{12}(\omega)$, for system with minimum cross-receptance function, $H_{12min}(\omega)$; point forcing, genetic algorithm optimization, $3 < m_i < 50$ kg, $0{\cdot}5 < \rho_{im} < 10{\cdot}0$ kg/m, $\omega = 10\,000$ rad/s, $b_1 = 0{\cdot}23L$. +, $H_{12min}(\omega)$.

first of these cases are given here; see Figures 28–30. The plot of the receptance function shows an extreme trough at the frequency of 10 000 rad/s chosen for the optimization. The finite, although small possibility, of finding ensemble members that give rise to such extreme behaviour indicates that the tails of the probability distribution functions describing the various response parameters will be extremely long. Clearly such an exercise, perhaps with use of more severe constraints for the ranges of parameters considered, might form a useful adjunct to SEA methods when considering extremal behaviour.

This process can be extended further by optimizing the integral of $H_{12}(\omega)$ with respect to ω on some chosen range. Such a calculation has been carried out here for the case of H_{12min} over the range 6000–14 000 rad/s, and the corresponding results are shown in Figures 31–33. From Figure 33 it can be seen that all the peaks have been reduced in magnitude when compared to those on either side of this range. In fact, a kind of "stop"

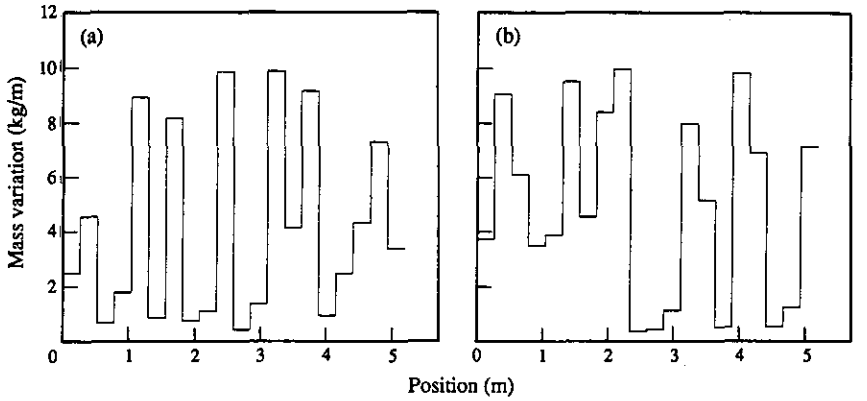

Figure 31. Mass profiles for system with minimum integrated cross-receptance function, $\min \int H_{12}(\omega)\,d\omega$; point forcing, genetic algorithm optimization, $3 < m_i < 50$ kg, $0{\cdot}5 < \rho_{im} < 10{\cdot}0$ kg/m, $\omega = 6000$–$14\,000$ rad/s, $b_1 = 0{\cdot}23L$. (a) Subsystem 1; (b) subsystem 2.

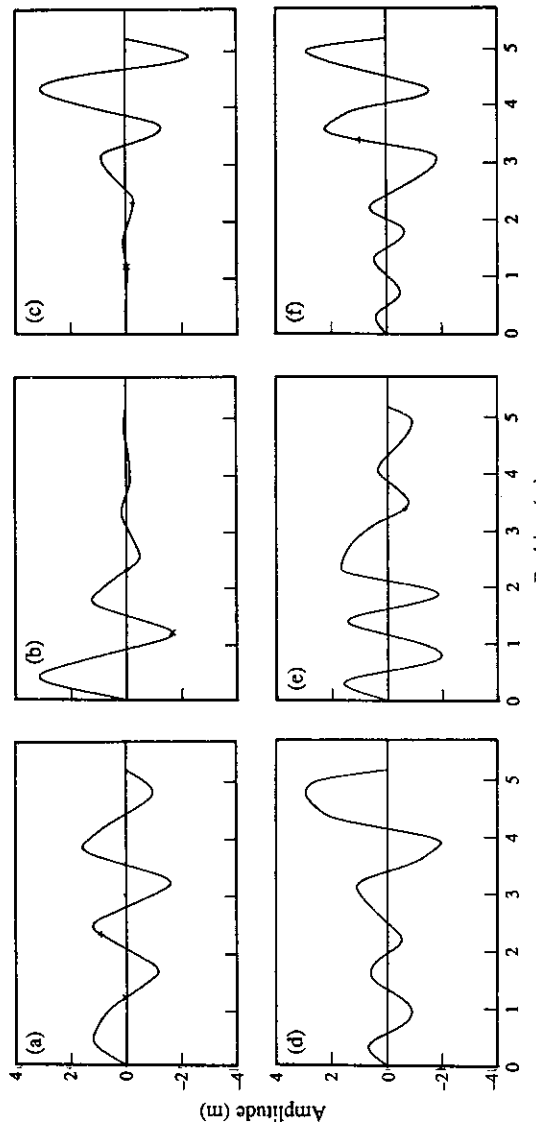

Figure 32. Mode shapes for system with minimum integrated cross-receptance function, $\min \int H_{12}(\omega)\,d\omega$ (axial variations show transverse for clarity); point forcing, genetic algorithm optimization, $3 < m_i < 50$ kg, $0{\cdot}5 < \rho_m < 10{\cdot}0$ kg/m, $\omega = 6000$–$14\,000$ rad/s, $b_1 = 0{\cdot}23L$. +, Coupling point; ×, drive point. Subsystem 1: (a) mode 6, 1·110 kHz; (b) mode 7, 1·340 kHz; (c) mode 8, 1·658 kHz. Subsystem 2: (d) mode 7, 1·377 kHz; (e) mode 8, 1·566 kHz; (f) mode 9, 1·709 kHz.

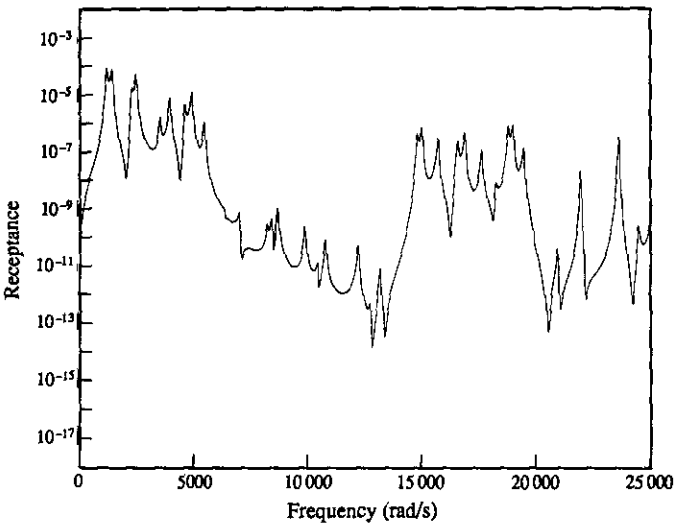

Figure 33. Deterministic cross-receptance function, $H_{12}(\omega)$, for system with minimum integrated cross-receptance function, $\min \int H_{12}(\omega)\, d\omega$; point forcing, genetic algorithm optimization, $3 < m_i < 50$ kg, $0{\cdot}5 < \rho_{im} < 10{\cdot}0$ kg/m, $\omega = 6\,000$–$14\,000$ rad/s, $b_1 = 0{\cdot}23L$.

band has been introduced into the receptance function. Such behaviour is, of course, well known in structures with periodic variations in physical parameters, and Figure 31 indeed demonstrates a tendency towards alternating light and heavy sections in the mass profiles. Moreover, the associated mode shapes show the localized large amplitudes characteristics of such nearly periodic systems [24].

It is clear from these studies that it is possible to modify dramatically the behaviour of a system by a choice of parameters which gives rise to suitable mode shapes and natural frequencies. However, the mass profiles used here are extremely unlikely to arise by chance if uniform rods are taken to be the equivalent deterministic case.

11. CONCLUSIONS

The random variability in energy flow characteristics of a system of two, coupled axially vibrating stochastic rods has been investigated by using computer simulation techniques. Attention has been focused on the input power receptance and coupling power receptance functions which are intimately connected with the definition of various SEA parameters. Exact analytical solutions for the PDFs of the input receptances are known to be possible for specific types of axially vibrating stochastic rods. These solutions have been used as benchmarks to validate the Monte Carlo simulation program.

The effects of different types of stochastic variations in subsystem properties on the probabilistic nature of the receptances have been investigated. The receptance functions are seen to show a statistically stationary behaviour beyond a cut-off frequency in most, but not all cases. This cut-off frequency is shown to be dependent on the spatial variation of the excitation, and also on the details of statistical modelling of system parameters. Contrary to expectations, the measures of dispersion associated with the responses are found not to reduce with increases in frequency. This feature may be associated with the constant modal densities and low modal overlap factors exhibited by the stochastic rod models used here.

Individual members of the statistical ensemble of vibrating systems, the responses of which deviate significantly from the average, have been identified and these illustrate the

extremes that may be found even with small parameter variations. Alternative schemes based on numerical optimization methods to generate systems showing even greater extreme responses have also been outlined. In these systems, not only the natural frequencies, but also the mode shapes, are shown to play a significant role in producing extreme responses.

It must be stressed that the systems studied here are very far from being general in nature, since most engineering problems of interest to practitioners of SEA consist of more than two subsystems, often with complex coupling topology and non-constant or high modal overlap factors. As such, this study represents part of an ongoing program of work directed at understanding the nature of the statistical variations in SEA predictions. Future publications will report on progress in this area and will address problems with more complex topology and, eventually, beam and plate based subsystems with higher and non-constant modal overlap factors.

ACKNOWLEDGMENT

This work has been supported by the U.K. Department of Trade and Industry.

REFERENCES

1. R. H. LYON 1975 *Statistical Energy Analysis of Dynamical Systems: Theory and Applications*. Cambridge, Massachusetts: MIT Press.
2. R. H. LYON and E. EICHLER 1964 *Journal of the Acoustical Society of America* **36**(7), 1344–1354. Random vibration of connected structures.
3. R. H. LYON 1969 *Journal of the Acoustical Society of America* **45**(3), 545–565. Statistical analysis of power injection and response in structures and rooms.
4. F. J. FAHY 1971 *Proceedings of the Seventh International Congress on Acoustics, Budapest*, 561–564. Statistics of acoustically induced vibration.
5. H. G. DAVIES and M. A. WAHAB 1981 *Journal of Sound and Vibration* **77**, 311–321. Ensemble averages of power flow in randomly excited coupled beams.
6. H. G. DAVIES and S. I. KHANDOKER 1982 *Journal of Sound and Vibration* **84**, 557–562. Random point excitation of coupled beams.
7. A. MOHAMMED and F. J. FAHY 1990 *Proceedings of the Institute of Acoustics* **12**(1), 543–550. A study of uncertainty in applications of statistical energy analysis to one-dimensional and two-dimensional structural systems.
8. C. H. HODGES and J. WOODHOUSE 1986 *Reports on Progress in Physics* (49), 107–170. Theories of noise and vibration transmission in complex structures.
9. T. A. BRODY, J. FLORES, J. B. FRENCH, P. A. MELLO, A. PANDEY and S. S. M. WONG 1981 *Review of Modern Physics* **53**, 385–479. Random matrix physics: spectrum and strength fluctuations.
10. R. L. WEAVER 1989 *Journal of the Acoustical Society of America* **85**(3), 1005–1013. Spectral statistics in elastodynamics.
11. H. G. DAVIES 1973 *Journal of the Acoustical Society of America* **54**(2), 507–515. Random vibration of distributed systems strongly coupled at discrete points.
12. A. J. KEANE and W. G. PRICE 1990 *Proceedings of the Institute of Acoustics* **12**(1), 535–542. Exact power flow relationships between many multi-coupled, multi-modal sub-systems.
13. C. S. MANOHAR and A. J. KEANE 1993 *Journal of Sound and Vibration* **165**, 341–359. Axial vibrations of a stochastic rod.
14. P. J. REMINGTON and J. E. MANNING 1975 *Journal of the Acoustical Society of America* **57**(2), 374–379. Comparison of Statistical Energy Analysis power flow predictions with an "exact" calculation.
15. A. J. KEANE and W. G. PRICE 1991 *Journal of Sound and Vibration* **144**, 185–196. A note on the power flowing between two conservatively coupled multi-modal sub-systems.
16. W. T. THOMSON 1965 *Vibration Theory and Applications*. New York: Prentice-Hall.

17. R. E. BORLAND 1963 *Proceedings of the Royal Society, London* **A274**, 529–545. The nature of the electronic states in disordered one-dimensional systems.
18. R. E. D. BISHOP and D. C. JOHNSON 1979 *The Mechanics of Vibration*. Cambridge University Press.
19. R. N. IYENGAR and C. S. MANOHAR 1989 *Transactions of the American Society of Mechanical Engineering, Journal of Applied Mechanics* **56**, 202–207. Probability distribution function of the eigenvalues of the random string equation.
20. C. S. MANOHAR and R. N. IYENGAR *Probabilistic Engineering Mechanics* (in press). Probability distribution of the eigenvalues of systems governed by the stochastic wave equation.
21. J. R. BENJAMIN and C. A. CORNELL 1970 *Probability, Statistics and Decision for Civil Engineers*. New York: McGraw-Hill.
22. C. H. HODGES 1981 TOP/14/81/1, *Topexpress Ltd, Cambridge, U.K.* Confinement of vibration by one-dimensional disorder: theory of ensemble averaging.
23. D. E. GOLDBERG 1986 *Proceedings of the* 1986 *Summer Computer Simulation Conference, Reno*, 44–48. A tale of two problems: broad and efficient optimization using genetic algorithms.
24. A. J. KEANE and W. G. PRICE *Journal of Sound and Vibration* **128**, 423–450. On the vibrations of monocoupled periodic and near periodic structures.